Characterization and Application of a Histamine Aptamer-Based Biosensor

by

Elysee Iraganje

MSc Candidate, Carleton University 2019

A thesis submitted to the Faculty of Graduate and Postdoctoral Affairs in partial fulfilment of the requirements for the degree of

Master of Science

In

Chemistry

Carleton University

Ottawa, Ontario

Abstract

Histamine is a biogenic amine, identified as a natural contaminant in food and alcoholic beverages, with high levels eliciting allergy-related conditions. Exposure to allergens can lead to abnormal high levels of histamine in the body that is detectable in blood and urine. A rapid histamine biosensor that can readily detect histamine levels in food, beverages and also be used as a diagnostic tool for allergy-related conditions will be an ideal point of care testing tool that is readily available at low cost. In addition, histamine has been identified as a close-range aggregation pheromone component in bed bug feces. Bed bug infestation has been on the rise in developed countries mainly in hotel, homes, shelters and school settings. A low cost, portable biosensor that readily detects bed bugs in these settings is in demand.

Nano-aptamer based biosensors have previously been used to detect wide range of targets in medical diagnosis, agriculture, and industry. In this study, selected histamine-binding aptamers (Hist_2, Hist_23, Hist_1min, Hist_2min, and Hist_23min) were characterized in solution with target histamine by a colorimetric binding assay and microscale thermophoresis. A head-to-head comparison of binding affinity and specificity for these group of aptamers were conducted, and the aptamer candidates best suited for biosensor application was selected. Aptamers Hist_2, Hist_23, and Hist_23min were selected out of the five aptamers due to their lowest LODs (400 nM, 600 nM, and 300 nM respectively) and high specificity towards target histamine through colorimetric binding studies. Further binding studies of these selected aptamers were conducted using microscale thermophoresis, and aptamers Hist_2 and Hist_23 were selected due to the observed specificity and strong affinity with K_D values of 1.29 μM and 68 nM, respectively towards the target. The aptamer candidate was further applied on an aptamer-based lateral

flow assay biosensor, that proved to be highly sensitivity with Hist_23 aptamer giving an apparent LOD of less than 10 nM.

Acknowledgements

I would like to first and foremost acknowledge my supervisor Professor Maria DeRosa for providing me the opportunity to be her graduate student in her remarkable lab. It was a privilege that I cannot take for granted. Professor Maria DeRosa was always supportive and encouraging throughout my time as her student. Her patient guidance and advice cannot be taken lightly, as these elements has made me a better researcher.

I would also like to express my sincere gratitude to all the kind-hearted students and staff in the DeRosa lab that welcomed and supported me. The close-knit group have all contributed to the unique, exceptional, loving experience I encountered in the lab. Among them, I am especially thankful for Dr. Velu Ranganathan, Dr. Sathya Srinivasan and Fiona Ebanks for their special guidance throughout my time as a student.

I am also indebted for the continual support of my parents, Dr. Euloge Baranjoreje and Dr. Aline Muryango. They have always cheered me on to achieve great things and their rallying motivation is what keeps me going to this day. I am also thankful for my siblings Esther Munezero, Joshua Mugisha, and David Niyukuri for always being there for me when I needed them most.

Lastly, I would also like to thank Carleton University, the Department of Chemistry, and the funding for providing me this unique opportunity to learn and excel in my academics.

Finally, as a young adult who is anchored to his faith, I cannot end without expressing my sincere gratitude to God, for His goodness and faithfulness.

Table of Contents

List of Tables

List of Figures

List of Appendices

List of Abbreviations

ASM	Aggressive SM
AuNP	Gold Nanoparticle
CM	Cutaneous Mastocytosis
Cy5	5’ Cyanine Dye
DAO	Diamine Oxidase
DMDS	Dimethyl disulfide
DMTS	Dimethyl trisulfide
DMT	4,4’-dimethoxytrityl
FA	Fluorescence Anisotropy
HNMT	Histamine-N-Methyltransferase
HPLC	High Performance Liquid Chromatography
H_1R, H_2R, H_3R	Histamine Receptor 1,2 &3
ISM	Indolent Systemic Mastocytosis
ITC	Isothermal Titration Calorimetry
LFA	Lateral Flow Assay
LSPR	Localized Surface Plasmon Resonance
MCL	Mast Cell Leukemia
MCS	Mast Cell Sarcoma
MST	MicroScale Thermophoresis
POC	Point of Care
QGRS	Quadruplex forming G-Rich Sequences
RIA	Radioimmunoassay

SELEX	Systematic Evolution of Ligands by Exponential Enrichment
SM	Systemic Mastocytosis
SM-AHNMD	SM-Associated Clonal Hematologic Non-Mast Cell Lineage Disease
SPR	Surface Plasmon Resonance
TEM	Transmission Electron Microscope

Chapter 1: Introduction

1.1 Histamine

Histamine is a biogenic amine with inflammatory and immunological functions [1]. It is synthesized from the decarboxylation of the amino acid histidine, catalyzed by the enzyme L-histidine decarboxylase as observed in **Figure 1.1.1**. Histamine is comprised of an imidazole ring attached to an ethylamine chain. Under physiological conditions, histamine is mainly protonated at the aliphatic amino group (pKa~ 9.4). The imidazole ring (pKa~5.8) exists in two tautomeric forms, in which either of the two nitrogen atoms is only protonated at a lower pH solution. Hence, this makes histamine a singly positively charged organic compound at neutral pH conditions [2,3].

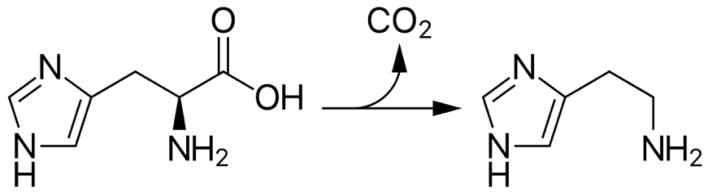

Figure 1.1. 1 Conversion of histidine to histamine by the enzyme L-histidine decarboxylase [4]

1.2 Histamine's role as a chemical signature for bed bug detection

The common bed bug *Cimex lectularius* infestation has been on the rise in developed countries due to increased international travel. Infestation is prevalent in hotels, trains, homes, cruise ships, schools, and homeless shelters [5,6]. Bed bug eradication has shown to be challenging due to increased resistance to insecticides. It is also difficult to apply insecticides onto and close to beds, as this will be harmful to humans. Heat treatments have been used to eliminate bed bugs however, this approach is expensive.

Bed bugs tend to cluster together in groups as a result of bed bug discharge of pheromones in their feces. Bed bugs release pheromones as soon as they identify safe shelters and a nearby food source, resulting in their occupation upon a surface as shown in **Figure 1.2.1**. Bed bug aggregation pheromone comprises of a blend of highly volatile components that includes dimethyl disulfide (DMDS), dimethyl trisulfide (DMTS), (*E)*-2-hexenal, (*E)*-2-octenal, 2-hexanone, and less volatile histamine component [7,8]. Studies have shown that bed bugs biosynthesize some pheromone components such as DMDS, DMTS, and histamine from amino acid precursors in human blood, namely DMDS and DMTS from methionine and histamine from histidine [8]. However, studies show that there are not enough precursors such as histidine in the blood to account for the high concentration of histamine that bed bugs excrete in their feces. It is therefore suggested that histamine, as well as other components are primarily biosynthesized *de novo* [8]. Histamine excreted in feces persist in household dust whereby environmental conditions such as sanitation, temperature, and humidity can influence its persistence [5].

Bed bug infestation has negative impact on human health and quality of life. Bed bugs feed on human host blood for survival and reproduction, with bed bug bites occasionally causing severe dermatitis [9]. Histamine deposited near where humans sleep, may result in breathing complications due to its proximity and persistence in our breathing spaces. There are also multiple mental health issues associated with bed bug infestations. Among them are psychological trauma, depression, anxiety, insomnia, and paranoia experiences [9,10].

Studies have shown that household dust from active bed bug infested homes had significantly higher histamine levels compared to un-infested homes. Bed bug infested homes consisted an average of 54 μg histamine/100 mg of dust (4.86 μM) or greater, compared to un-infested homes that consisted an average of less than 2.5 μg/100 mg of

dust (0.23 μM) [5]. There is a clear association between high levels of histamine in household dust and the presence of bed bugs.

Proactive early detection of bed bugs is critical to prevent infestation from spreading rapidly. However, at low infestation levels, it is difficult to detect them due to their tendency to hide in concealed areas. The current methods that are commonly used to detect bed bug infestation, includes visual inspection, passive and active monitoring devices, and the use of canines trained to find bed bugs. However, these methods have low detection accuracy at early infestation stages. They are also deemed time consuming, expensive, and require skilled operators [9,10]. Recent development of a lateral flow device that detects bed bug residue, has proved to improve the detection accuracy of bed bugs [9]. Moreover, novel bed bug proteins (BBP1 and Egg shell protein) identified have been used to make an antibody-based detection assay that exhibited a high sensitivity [6] . With histamine being identified in bed bugs, a portable, easy-to-use biosensor able to specifically detect histamine as a surrogate for bed bugs could be highly desirable. The biosensor would need to be inexpensive and not require bulky instruments nor skilled operators, enabling it to be introduced in settings with high infestation rate such as hotels, homeless shelters, and schools.

Figure 1.2. 1 Bed bugs infestation. Photo illustrating a typical bed bug aggregation on a mattress [11].

1.3 Histamine's role in Anaphylaxis and Chronic Mastocytotic Conditions

1.3.1 Anaphylaxis

Anaphylaxis is a severe hypersensitive reaction that the World Allergy Organization considers as life-threatening and even fatal [12,13]. The Anaphylaxis Network Symposium of the United States considers it a serious allergic IgE mediated reaction that is often life-threatening [12,14]. It can be defined as an acute, suddenly occurring reaction that generally happens in the skin and mucosal tissues [15]. However, anaphylaxis is generally accepted as a relatively rare condition, with a lifetime prevalence approximately calculated to be 0.05-2.0 %, of which about 1 % of cases are fatal [12,15].

Anaphylaxis reaction occurs when mediators such as histamine, tryptase, heparin and chymase are released from mast cells. The release of these mediators will trigger major symptoms observed in the skin such as, urticaria (also known as hives), angioedema and flushing [12]. Other symptoms are also observed in mucosal tissues such as swelling of the tongue. The GI tract is also affected, with symptoms that include abdominal cramps, vomiting and diarrhea. The respiratory tract and cardiovascular system are among the

systems affected with individuals showing symptoms that includes dyspnea, wheezing, hypoxemia and low blood pressure [12].

Anaphylaxis are mainly triggered by specific dietary intake, specific drugs, and Hymenoptera venoms. Such common examples of food intake that triggers an anaphylaxis include peanuts, seafood, milk, and vegetables. Drugs such as antibiotics, general anesthetics, antirheumatics and many others are also major contributors to the cause of anaphylaxis [12]. Typical causes of anaphylaxis well known to the general population are stings from Hymenoptera venoms such as honeybees and vespids.

1.3.2 Mastocytosis

Mastocytosis is an increasingly prevalent condition associated with an elevation of mast cells in the skin and/or internal organs such as, the bone marrow, GI tract, liver and lymph nodes [15-17]. The release of mast cell mediators such as histamine, tryptase and chymase will result in multiple symptoms i.e. hives, nausea, diarrhea, abdominal pain, difficulty in breathing and hypotension [15,17].

Mastocytosis possesses a somatic gain-of-function mutation in the KIT receptor tyrosine kinase, commonly in codon 816 (D816V), whereby valine is substituted for an aspartate in the second catalytic domain [17,18]. The D816V mutation causes the KIT receptor to be continually active, independent of stem-cell factor, resulting in autophosphorylation that leads to enhanced survival and cell autonomous growth of mast cells [18,19]. This mutation is detectable in more than 90 % of patients with mastocytosis [17].

According to the World Health Organization, mastocytosis has seven variant forms. This includes: Cutaneous Mastocytosis (CM), Indolent Systemic Mastocytosis (ISM), SM with an associated clonal hematologic non-mast cell lineage disease (SM-AHNMD), aggressive SM

(ASM), mast cell leukemia (MCL), mast cell sarcoma (MCS), and extracutaneous mastocytoma [12,20].

CM is most prevalent in children with symptoms that includes mainly skin lesions [12]. It is diagnosed in the first years of life and characterized by multiple hyperpigmented macular that become urticarial when scratched. However, it has a good prognosis as their condition improves or resolved as they go through puberty [19]. Adult onset is usually associated with SM, with the bone marrow being involved in all SM patients. In patients with SM, mast cells infiltrate in various internal organs, including the bone marrow, spleen, liver and GI tract. ISM is a slowly progressive disease, that is prevalent in adults. Patients with ISM show no severe symptoms and the disease is easier to treat [12]. However, there are other rare severe forms of mastocytosis such as SM-AHNMD, ASM, MCL, and MCS that are rapidly progressing with fatal outcomes. SM patients exhibits variable clinical outcome, ranging from asymptomatic cases to swiftly fatal cases [12,21].

Previous studies have indicated a strong association between anaphylaxis and mastocytosis, with the prevalence of anaphylaxis being reported in 20-56 % in adults, and 6-9 % in children patients with mastocytosis [12,15,16]. Anaphylaxis risk in children with CM was shown to be higher compared to the general population. Moreover, anaphylaxis is significantly more common and severe in adults with SM compared to those with CM. Studies have shown that 50 % of patients with SM reportingly experience severe anaphylaxis reactions [12,15,17]. The main reason why anaphylaxis is severe in patients with mastocytosis compared to the general population, is due to increased release of mediators such as histamine from mast cells [12]. Over the years, severe or even fatal cases of anaphylaxis with mastocytosis have been reported. Moreover, human exposure to allergens such as Hymenoptera venom stings in patients with mastocytosis, have previously resulted

in severe or even fatal anaphylaxis reactions. Other studies have also shown that other allergens, such as foods and drugs have caused severe or harmful anaphylaxis reactions in patients with mastocytosis [12].

Treatment of anaphylactic reactions from mastocytotic patients come in different forms. Firstly, all patients with mastocytosis are advised to avoid substances and environments that may trigger mast-cell activation. They should also carry two to three epinephrine self-injectors and use them in emergency situations [19]. In addition, anti-mediator drugs are prescribed for all patients with mastocytosis who are suffering from chronic and frequent mast cell activation symptoms. HR1 antihistamine blockers in combination with or without HR2 antihistamine blockers are the basic prescription of all patients with mastocytosis [12,22]. Patients with gastrointestinal symptoms (such as abdominal cramps), or those that do not respond to HR1 blockers alone are prescribed with HR2 blockers [22]. Moreover, there are also drugs that interfere with mast cell activation, proliferation, survival and mediator release that have shown to be effective [19]. These drugs include Ketotifen that inhibits the activation of mast cells, while Glucocorticosteroids and Cyclosporine-A inhibits the production of mediators [22]. Immunotherapy drugs such as Cladribine (suppresses the immune system) are prescribed only to patients with ASM, MCL or patients with high risk of life-threatening anaphylaxis. There have also been gene therapy studies that have attempted to develop drugs that targets the KIT D816V mutation, which is a mutation that is critically involved in the pathogenesis of mastocytosis [23].

Current diagnosis of anaphylaxis in patients with mastocytosis are through the detection of biomarkers. High levels of inflammatory mediators are released from mast cells into the blood stream and excreted in urine. Currently, there are commercial immunoassays present that allows for the detection of these mediators (tryptase, histamine, n-methylhistamine

etc) in the blood stream and urine [18,24]. Commercial kits that allows the detection of these mediators include ELISA kits and radioimmunoassay (RIA) techniques [24,25].

1.3.3 Histamine as a Mediator

One of the mediators released from mast cells that elicits allergic reactions is histamine. Histamine is secreted and stored by both mast cells and basophils upon immunological and non-immunological activation [1]. Mast cells are abundant around areas prone to injury such as nose, mouth, and blood vessels. Histamine release from mast cells occurs when allergens bind to mast-cell-bound IgE antibodies. Once released, histamine stimulates different biological response through tissue-specific expression of four major histamine receptors; H_1R, H_2R, H_3R, or H_4R as illustrated in **Figure 1.3.3.1** [1,3]. Stimulation of H_1R elicits contraction of smooth muscle of the respiratory tract and increases vascular permeability, resulting in symptoms such as urticaria, broncho-constriction, and hypotension. H_2R are found on parietal cells located in the stomach lining. Parietal cells are responsible for regulating gastric acid levels, that is released upon stimulation of H_2R. Symptoms that results from the release of gastric acid includes abdominal cramps, vomiting and diarrhea. H_2R are also found on the heart, uterus and vascular smooth muscle cells, where stimulation of these receptors results in smooth muscle relaxation [26]. Furthermore, H_3R are found in the central nervous system, whereby they regulate histamine levels in the body as well as other important neurotransmitters. Lastly, the H_4R mainly regulates the level of white blood cells in the body and are located in the thymus, spleen, bone marrow and basophils [27].

In the aftermath of an anaphylaxis reaction, histamine blood concentration levels rise within 10 minutes of the start of the symptoms, and later returns to normal within 30-60

minutes. It is rapidly metabolized by methylation of the imidazole ring by histamine-N-methyltransferase (HNMT) into n-methyl histamine, or by oxidative deamination of the primary amino group by diamine oxidase (DAO) into imidazole acetaldehyde [1,28]. The rise in histamine levels and its metabolites are also detected in the urine [25,29,30]. As mentioned in **Table 1.1**, the normal histamine concentration in the blood is approximately 4.01 nM, while normal histamine levels in urine is approximately 0.21 μmol/24 h [28,31,32]. As an anaphylaxis reaction occurs, the histamine blood concentration rises to around 13.50 nM, while histamine levels in urine also increases to around 1.8 μmol/24 h as stated in **Table 1.1** [28,32,33].

Several techniques are readily available for the detection of histamine as briefly discussed earlier. Most common are commercial ELISA kits, which detect histamine in plasma and whole blood samples with LODs of 1.08 nM and 1.79 nM, respectively [34,35]. Currently, there are non-invasive histamine ELISA kits that detects histamine levels in urine collected over 24 hours with an LOD of around 2.70 nM [34]. However, the use of antibodies to prepare ELISA kits is expensive, and they also exhibit cross-reactivity with other biogenic amines [1,36]. Other non-invasive techniques include high-performance liquid chromatography (HPLC) and HPLC coupled to mass spectrometry [1]. Unfortunately, these techniques are also expensive and require specialized laboratory settings.

A rapid and cost efficient sensitive diagnostic tool is desired to detect the abnormal high levels of histamine concentrations in the body in the aftermath of an anaphylaxis reaction and in patients with mastocytosis. Specificity and rapid detection would be required to develop a medical diagnostic tool for the quick diagnosis of mastocytosis and anaphylaxis reactions. Such biosensor will also need to be cheap and not require bulky instruments nor

skilled operators, which is important for a point of care (POC) diagnostic tool to be readily available to the general public including in remote areas.

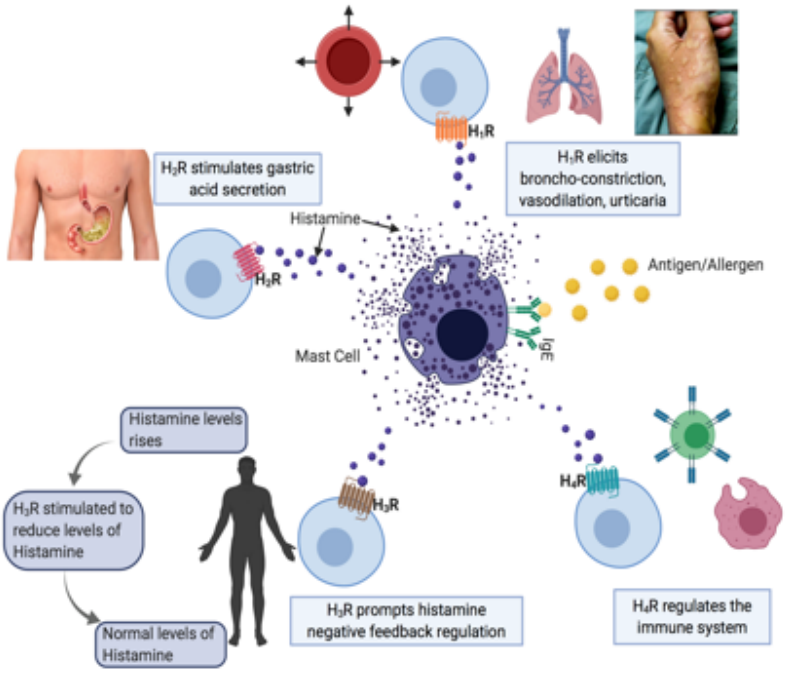

Figure 1.3.3. 1 Schematic illustration of an allergic IgE mediated reaction, that results in the release of histamine from mast cells. Histamine released will bind on H_1R, H_2R, H_3R, or H_4R eliciting multiple symptoms and biological reactions in the body [26,37,38]. *Figure was designed on BioRender*.

Table 1. 1 Contrasting differences between normal and abnormally high histamine concentrations in blood and urine samples in the aftermath of an allergy reaction [28,31-33]

Biological Fluid	**Normal Histamine Concentration**	**Abnormal Histamine Concentration**
Blood	4.01 nM	13.50 nM
Urine	0.21 µmol/24 h	1.80 µmol/24 h

1.4 Biosensor for Detection of Histamine in Food and Beverages

Histamine is naturally found at low levels in food, particularly seafood, meat, cheese, fruits and vegetables. Histamine is also found in fermented drinks such as beer and wine [3,39,40]. Histamine is derived from the decarboxylation of free histidine amino acid that is naturally found in food and sometimes released from proteins as a result of proteolytic cleavage. Histidine decarboxylase-positive microorganisms convert amino acid histidine to histamine and are naturally associated with the food or maybe introduced by contamination during food processing. In fermented foods and beverages, the applied starter cultures affect the production of histamine [39].

Minimal concentrations of histamine found in food and drinks is considered non-toxic. However, as the food becomes spoiled, the amount of histamine increases to a toxic level, prompting food poisoning. Food spoilage sets up favorable conditions for growth of decarboxylase-positive microorganisms that are highly enzyme active. The growth of such bacterial species includes, *Morganella psychrotolerans*, *Morganella morganii*, *Klebsiella pneumoniae*, and *Proteus vulgaris* which have been found in spoiled food with elevated histamine levels [3]. The microbial spoilage of food is accompanied by the increase production of decarboxylases, hence elevating histamine levels in food [39]. High concentration of histamine in food such as fish is also associated with proteins and free histidine amino acids that are abnormally high, due to the increased protease enzymatic activity produced by contaminant bacteria [3]. According to Health Canada, the established maximum allowable levels for histamine contaminants in food is 100-200 mg/kg and is routinely enforced by the Canadian Food Inspection Agency. The FDA and European food regulations require maximum histamine levels to not exceed 50 mg/kg and 100 mg/kg,

respectively [40]. Other countries have similar upper limits of 100 mg/kg histamine in foods, and 2 mg/L of histamine contaminants in alcoholic beverages [39].

Conventional prevention of histamine formation in food includes the limitation of bacterial growth through chilling and freezing. Histamine production is slowed down at 10℃ and minimal traces are produced at 5℃, due to the destruction of histidine decarboxylase-positive bacteria. The presence of alkaline medium also prevents growth of these decarboxylase bacteria due to their optimal activity at low pH in the range of 2.5-6.5 pH [39]. Other alternative approaches that lower histamine levels in food includes, hydrostatic pressure, irradiation, and food additives. In alcoholic beverages, enzymes that can readily degrade histamine such as diamine oxidase (DAO), are added to starter cultures during fermentation [3].

As soon as humans ingest histamine, the human detoxification system responds by rapidly metabolizing histamine into n-methyl histamine by HNMT or into imidazole acetaldehyde by DAO, which are less active products with minimal to no effect to the body. However, if the detoxification system fails to cope with the high levels of histamine ingested, histamine binds to the readily available histamine receptors (H_1R, H_2R, H_3R, or H_4R) inducing an allergic reaction. Typical symptoms that result from histamine intoxication are hypotension, bronchoconstriction, urticaria, and nausea.

It is imperative to have a reliable detection method for histamine analysis in food and beverages. Currently, there are common and emerging histamine detection techniques. These methods include instrumental analysis using mass spectrometry and HPLC, offering high sensitivity. However, these are time consuming and expensive sophisticated instruments that require highly skilled labor, which is not ideal for everyday food testing [40, 41]. Biosensor method are also emerging as histamine detection techniques that provide a

good alternative to traditional methods due to low cost, rapidity, and no need for skilled operators. Current biosensor techniques include enzyme assays and electrochemical sensors [3]. However, there is a persistent need for a highly specific, rapid, and low-cost histamine detection assay for food and beverage testing.

1.5 Aptamers

Aptamers are artificial single-stranded oligonucleotides that can bind to specific target molecules with high affinity and specificity. Aptamers have advantages over antibodies, in that they are oftentimes more specific, and efficient in binding diverse small targets. Such targets include, drugs, mycotoxins, amino acids, pesticides, proteins and whole cells [42,43]. Moreover, aptamers are more chemically stable and effective in a wider range of solutions and conditions [44]. Aptamers are also easily produced in bulk quantities with less batch-to batch variation, within a short period of time and at a low cost, while antibody creation is a lengthy and costly process [45,46]. Aptamers have been and are currently being used for diagnostic, therapeutic and bioanalytical applications in medicine, agriculture and industry settings [47]. Aptamers are derived from an in vitro selection production, referred to as SELEX (systematic evolution of ligands by exponential enrichment). Initially, a random single-stranded oligonucleotide library is synthesized. The library then undergoes repetitive cycles of incubation with the target, followed by the recovery of bound oligos, and then enrichment by PCR amplification [47].

The ability of aptamers to undergo conformational changes upon target binding, as well as their specificity and low cost, are key reasons why they have been used in various types of biosensors, such as electrochemical, fluorescence, colorimetric assays, and surface plasmon resonance (SPR) techniques [48,49]. AuNP colorimetric based sensors have been

widely applied in real- time-on-site monitoring and rapid testing of food quality and safety, as this sensor is simple, rapid, and highly sensitive [41]. In this study, a DNA histamine aptamer-based colorimetric biosensor was developed. The histamine aptamers were initially selected by several groups including Mairal Lerga et al, John Ho et al, and the DeRosa group (Valenzano, McKeague, DiGirolamo, DeRosa, unpublished) [36,50].

Firstly, binding characterization studies were conducted on aptamers Hist_2, Hist_23, Hist_1min, Hist_2min, and Hist_23min. Aptamers Hist_1min, Hist_2min and Hist_23min are truncated minimers of full-length aptamer sequences. Aptamers Hist_2 and Hist_23 are all 71 base full-length sequences, consisting of primer regions as well as 40 base length randomized regions while, the minimers only consists of the 40 base length randomized regions. In this experiment, a head-to-head comparison of binding affinity and specificity for these group of aptamers were conducted, and the aptamer candidate better suited for a biosensor assay was selected. This histamine aptamer-based colorimetric biosensor can be utilized in different areas such as in medical diagnosis of allergy conditions, detection of bed bugs, and histamine detection in food and alcoholic beverages.

Thesis Objective

The objective of this study was to determine and identify potential histamine aptamers that are capable to bind to target histamine with high affinity and specificity. Characterization of histamine aptamers were conducted through in-solution colorimetric binding assays, whereby the specificity and LODs of each aptamer were determined. Further characterization of histamine aptamer interaction in solution was conducted through MicroScale Thermophoresis (MST) to determine the K_D of the histamine aptamers. The

potential histamine aptamers that showed ideal binding characteristics were selected for further biosensor studies.

Chapter 2: Preparation and Characterization of Aptamers through Colorimetric Binding Studies and MicroScale Thermophoresis

Statement of Contribution

TEM images for aptamer-AuNPs colorimetric binding studies were performed by Dr. Jianqun Wang at Carleton University. MicroScale Thermophoresis experiment was performed by Dr. Thomas Schubert at 2bind Molecular Interactions inc (Regensburg, Germany).

2.1 Characterization of Aptamer Interactions in solution using Colorimetric Binding Assay

Metal nanoparticles such as gold nanoparticles (AuNPs) have been used extensively in a variety of biosensor assays for analyte detection. AuNPs unique high extinction coefficient (e.g. for a 14nm ε= 2.42E8 $M^{-1}cm^{-1}$) that depends on their physical and distance-dependent properties, accounts for their high sensitivity enabling them to have extensive applications in biosensing assays [51-53]. The dramatic change in color can easily be monitored with the naked eye, which provides a simple and cost-effective methodology in bioassays [54]. Common applications of AuNPs in biomedical research includes electrochemical biosensors, drug delivery, immunoassays and detection of various targets [52].

One major property that AuNPs possess is the unique localized surface plasmon resonance (SPR) that are confined onto individual nanoparticles. When AuNPs are exposed to light, the electromagnetic field of light induces a collective oscillations of electrons, giving rising to SPR [53,55]. Localized SPRs enhance the electric field near the surface of the nanoparticles, with its highest enhancement at the nanoparticle surface and rapidly decaying thereafter [56,57]. Its unique localized SPR depends on the particle size, shape, and inter-particle distance which is responsible for the color of AuNPs [53]. Thus, dispersed

AuNPs with sizes of 10-50 nm are red in color and exhibit a maximum absorption wavelength at 520 nm. When AuNPs aggregate as a result of van der Waals attractive forces, the color changes to purple-blue and the maximum absorption wavelength increases to 610-670 nm [41,52-54]. AuNPs are conventionally characterized with transmission electron microscope (TEM) and UV-vis spectrometry to determine the size, shape and concentration [58].

In the AuNP colorimetric assay, upon the addition of target, AuNPs aggregate in the presence of salt that results in a color change from red to blue. As the distance between the nanoparticles decrease, near-field coupling starts to occur, resulting in a stronger enhancement of the localized electric field within the particle-particle spacing. This results in a red shift of the maximum absorption wavelength to 630-670 nm [41,51,54,59,60]. The intensity of the color change is dependent on the concentration of analyte [57]. The AuNP solution changes color from red to purple-blue as the concentration of analyte increases. Increased aggregation is characterized by a gradual decrease of the absorption peak at 520 nm and the appearance of a new peak at 630 nm [54].

The aptamer-based colorimetric assay is a simple, fast, and relatively inexpensive detection method, with results visible with the naked eye [52,53]. Due to its adaptability, high sensitivity, and versatility, aptamer-based colorimetric assays have widely been applied for the detection of proteins, nucleic acids, viruses, bacteria and toxins [47,53,61-64]. Conventionally, aptamers are adsorbed onto the citrate-coated AuNP surfaces via the nitrogenous bases of the DNA, resulting in a well dispersed AuNP-aptamer conjugate red solution in the presence of salt. Upon the addition of target, the target induces the conformational change within the aptamer which leads to the desorption of aptamers from the AuNPs surface, as the aptamers preferably interact with target. Consequently, this leads

to the aggregation of AuNPs in the presence of salt, with the color of the solution changing to purple-blue [43,44,51]. In this study a “reverse adsorption-desorption” colorimetric approach is introduced as illustrated in **Figure 2.1.1**, whereby aptamers are initially incubated with target histamine, followed by the incubation of mixed solution with AuNPs. In the presence of histamine target, aptamers are unable to passivate the AuNP surfaces, as they preferably bind specifically onto histamine target, resulting in a solution color change from red to purple-blue upon salt addition.

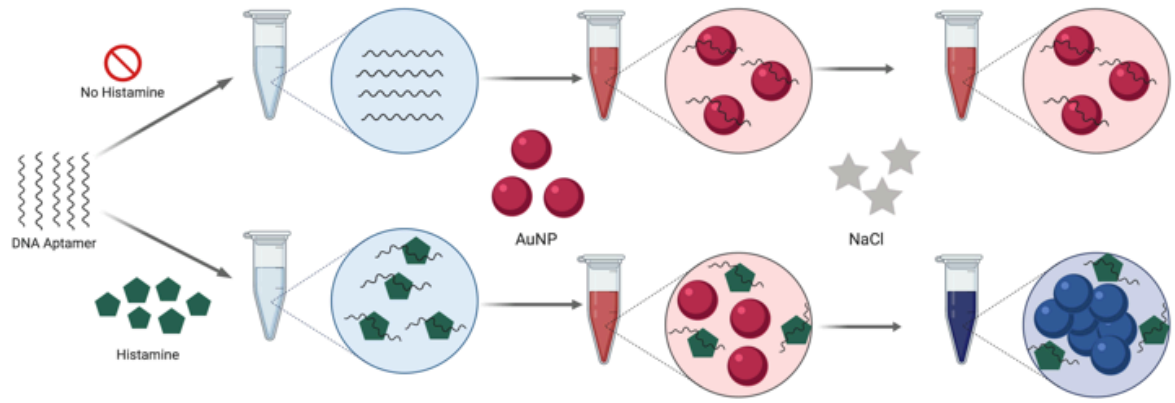

Figure 2.1. 1 Schematic illustration of reverse adsorption-desorption colorimetric method. Aptamers are initially incubated with or without target histamine, followed by the incubation of solution with AuNPs. Salt induced AuNP aggregation occurs when aptamers preferably bind to target histamine, resulting in a solution color change from red to blue. *Figure was designed on BioRender*.

2.2 Characterization of Aptamer Interactions in solution using Microscale Thermophoresis (MST)

Further aptamer binding studies are necessary to determine their affinity and specificity. There are multiple techniques that have been used to study aptamer interaction with target. These methods include SPR, Isothermal Titration Calorimetry (ITC), Fluorescence anisotropy (FA) and many other techniques. In this experiment, MST was used to characterize aptamer interactions in solution. The rapid measurements and low sample consumption use makes MST an ideal aptamer characterization method [47].

MST technology takes advantage of the physical properties of the molecules being studied. These molecules move in temperature gradients depending on their size, charge, and hydration shell. In this experiment, the molecules characterized are the histamine aptamers. Upon the aptamer interaction with the target histamine, a change in at least their size, charge, or hydration shell physical property will occur, resulting in an altered thermophoretic mobility of the aptamer. Each aptamer has a unique "thermophoresis" that can be measured. The dissociation constant K_D (measures affinity of molecules) of the aptamer can be determined by monitoring the fluorescence of the movement of the interacting labelled aptamer-target complex [47,65].

In this experiment, the aptamers characterized are labelled with a Cy5 fluorescence dye on the 5' end. As the aptamer interacts with the histamine target, the fluorescence signal of the Cy5 fluorescence dye is monitored. Initially, the fluorescence of the aptamer in solution with ligand is measured without the temperature gradient to ensure homogeneity of the sample. As observed in **Figure 2.2.1**, activation of an IR laser results in the initiation of a temperature gradient. Within this temperature gradient, an initial steep drop of the fluorescence signal is observed known as the T-Jump, whereby the fluorescently labelled

aptamer in bound and unbound state rapidly diffuse away from the heated region. This is followed by a slower depletion of fluorescence driven by the thermophoretic movement of fluorescently labelled aptamer in bound or unbound state, which exhibit differentiated fluorescence intensity depending on the concentration of ligand until a steady state is reached. As the IR-laser is deactivated, a reverse T-jump is observed whereby the fluorescent labelled aptamers diffuse back [65]. The K_D is determined by preparing a serial dilution of the target histamine, mixed with a constant concentration of fluorescent labelled aptamers [65]. By determining the K_D of the histamine aptamers, one can select the aptamer with the highest affinity as the most suitable aptamer to conduct further binding studies.

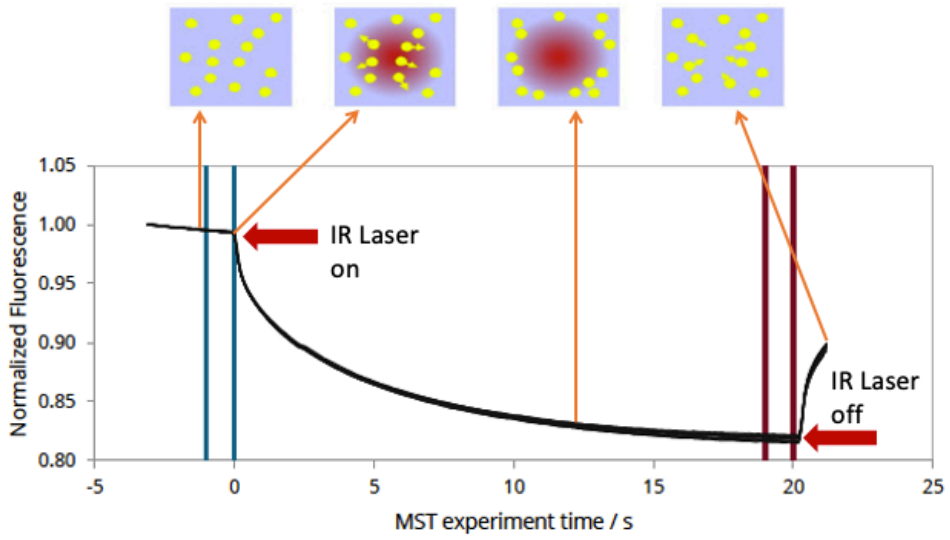

Figure 2.2. 1 An MST time trace of capillaries containing a constant concentration of fluorescently labelled aptamers and an increasing concentration of interacting ligand, showing a movement profile of molecules in a temperature gradient. Initially there is a cold phase (laser off) for a couple of seconds. The laser is then switched on and initiates a T-jump phase, in which the temperature gradient is established. The fluorescent dye decreases its signal intensity upon heat induction, and the thermophoretic movement of fluorescently labelled interacting aptamers takes place. After a couple of seconds, the IR-laser is deactivated, and a reverse T-jump is observed whereby the fluorescent labelled aptamers diffuse back [65].

Chapter Objectives

The objectives of this chapter were to synthesize histamine full length aptamers and truncated minimers. These aptamers were characterized by in-solution colorimetric binding assays and microscale thermophoresis. The best candidate aptamers were selected towards to make a strip test.

Chapter 3: Materials and Methods

3.1 Materials and Instrumentation

Gold (III) chloride hydrate ($HAuCl_4.3H_2O$, ≤99.9%), sodium citrate, sodium chloride, histamine (2-(4-Imidazolyl) ethylamine, ≥97.0%), 4-dimethylaminopyridine, 2-acetyl pyrrole, L-Histidine monohydrochloride monohydrate, L-tryptophan, and Indole were purchased from Sigma-Aldrich. Ultrapure water was obtained from a Millipore Milli-Q deionized water system at 18 MΩ (Waters, Milford, MA, USA). HR TEM images were recorded using a FEI Tecnai F20 FETEM. Chemistry UV/Vis absorption spectra were obtained using a CARY 300 Bio spectrophotometer (Varian, USA). A high-speed Sorvall legend micro 21R (Thermo electron corporation) centrifuge was used for the centrifugation of the solutions.

3.2 Aptamer Synthesis for Colorimetric Assay

Histamine aptamer sequences Hist_1min, Hist_2min, Hist_23min, Hist_2 and Hist_23 were prepared using standard phosphoramidite chemistry on a Bioautomation MerMade 6 DNA synthesizer (Plano, TX, USA). Oligonucleotides were synthesized in a 3’ to 5’ direction through a repeating series of solid phase organic reactions (Glen Research). Hist_2 and Hist_23 sequences were all 71 based length aptamers containing identical 3’ and 5’ primer

binding regions, and a randomized region as indicated in **Table 3.1**. Aptamers Hist_1min, Hist_2min, and Hist_23min sequences only contained randomized region and no primer binding regions were present.

The phosphoramidites, dA-CE, Ac-dC-CE, dmf-dG-CE, and dT-CE were obtained from Glen Research (Sterling, VA, USA). They were each dissolved in anhydrous acetonitrile (Glen Research) to create 0.1 μM solutions of each amidite in argon atmosphere. Ultra-High Purity 5.0 argon was purchased from Praxair Canada (Mississauga, ON, Canada). The dissolved phosphoramidites were connected to the DNA synthesizer along with anhydrous acetonitrile (BDH VWR analytical), activator solution, deblock solution, cap A solution, cap B solution, and oxidizer solution which are all obtained from Glen Research (Sterling, VA, USA). The 1000 Å 1.0 μmole-controlled pore glass synthesis columns (Bioautomation) for Hist_2 and Hist_23 aptamers contained an initial thymine, while Hist_1min and Hist_23min contained an initial cytosine, and Hist_2min contained an initial guanine. The appropriate script file was loaded on the MerMade software and synthesis was performed overnight.

Table 3. 1 Lengths of each aptamer sequence. Theoretical extinction coefficients of each aptamer sequence were determined with OligoAnalyzer® Tool, version 3.1.

Sequence Name	**Length (bases)**	**Extinction Coefficient at 260nm (L mol^{-1} cm^{-1})** [66]
Hist_2	71	705500
Hist_23	71	696400
Hist_1min	40	392500
Hist_2min	40	401700

Hist_23min	40	392300

*Histamine aptamers were selected by Valenzano, McKeague, DiGirolamo and DeRosa, unpublished work.

3.3 Purification of Synthetic Oligonucleotides

Following DNA synthesis, the 4,4'-dimethoxytrityl (DMT) oligonucleotide was deprotected in 1 mL of ammonium hydroxide at 65℃ for 2 hours. Once cooled at room temperature, a 1 mL of 100 mg/mL sodium chloride solution was added to the deprotected DMT-ON oligonucleotide for a final volume of 2 mL. The 150 mg Glen-Pak DNA Purification Cartridges (Glen Research) were conditioned using 0.5 mL of acetonitrile followed by 1 mL of 2 M TEAA on the vacuum pump. The acetonitrile washes organic residues from resin, while the TEAA acts as an ion-pairing reagent to enhance the binding of the DMT-ON oligonucleotide to the resin. The oligo/salt mixture was applied onto the cartridge in 1 mL aliquots. During the loading process, the DMT-ON oligos are bound to the cartridge, while failure sequences are not retained. The cartridge was then washed with 2 x 1 mL of salt wash solution (5 % Acetonitrile in 100 mg/mL Sodium Chloride) to wash away the remainder of the failed sequences from the cartridge. This was followed by the rinsing of the cartridge with 2 x 1 mL of 2 % TFA to remove the DMT from the bound oligonucleotide. The cartridge was then washed with 2 x 1 mL of deionized water, rinsing away the TFA and excess salts. The purified oligos were eluted into sample tubes using 1 x 1 mL 50 % acetonitrile in water with 0.5 % ammonium hydroxide. The collected oligos were dried down by a SpeedVac overnight; an Automatic Environmental SpeedVac® System AES2010 (Savant).

3.4 Quantification of Aptamers using UV-Vis Spectroscopy

Synthesized DNA concentration was determined using UV-Vis spectroscopy using a CARY 300 Bio spectrophotometer (Varian, USA). Aliquots of the DNA stock solutions were diluted with deionized water, in order to measure absorbances between 0.4-0.8 at 256 nm. The Beer-Lambert Law equation was used to determine the concentration of each aptamer using the measured absorbance value and the theoretical extinction coefficient, provided through the use of OligoAnalyzer® Tool, version 3.1, on the Integrated DNA Technologies (IDT) website (PrimerQuest® program, IDT, Coralville, Iowa, USA).

The purity of the aptamer was determined through molecular weight verification by mass spectrometry. Samples of 1 nmol of the aptamer solution were dried using the SpeedVac and sent to McGill University for LC-MS analysis.

3.5 Secondary Structure Prediction of Aptamers

The secondary structures of the aptamers were predicted using RNAstructure[90], version 6.0.1, from the Matthews lab, to determine the minimum free energy structure of the aptamer sequences. The online tool was set to DNA and all other options were left at the default settings.

Furthermore, using the Standard Nucleotide BLAST® online software, the aptamers were analyzed to determine if any of the aptamers are likely to be in the same sequence family. Moreover, potential G-quadruplex structures were analyzed in all aptamers using QGRS (Quadruplex forming G-Rich Sequences) Mapper software.

3.6 Preparation of Gold Nanoparticles

All glassware were prepared by washing with Aqua Regia (3:1 of HCl:HNO_3) followed by rinsing with deionized water. A volume of 98 mL of deionized water and 2 mL of 50 mM $HAuCl_4$ was mixed for a final concentration of 1 mM $HAuCl_4$. The solution was heated to boiling with magnetic stirring, while flask was covered with aluminum foil. Upon boiling, 10 mL of 38.8 mM sodium citrate was added to the solution, resulting in a gradual change in suspension color from yellow to clear, then to purple and finally to red. Nanoparticle solution was allowed to cool at room temperature and stored in a fridge. AuNPs were then quantified by UV-Vis spectrometry.

3.7 Preparation of the Colorimetric Assays

A series of salt and aptamer optimizations were initially conducted to determine the concentrations of NaCl and aptamer required for the colorimetric assay experiment. This was followed by a histamine target control experiment that determines any false positives, whereby AuNP solutions were incubated with increasing concentration of target histamine (1 nM-1500 nM).

Furthermore, the aptamer binding target colorimetric assay was conducted. Aptamer (8 µL of 10 µM stock in water) was added to histamine target prepared in water at final concentrations ranging from 1 nM to 1.5 µM and incubated for 30 minutes. This was repeatedly carried out with all histamine aptamers synthesized. AuNP (50 µL aliquot of 11.77 nM solution) was added into each microcentrifuge tube and vortexed briefly, followed by a 30 minutes incubation period. A final concentration of 0.041 M NaCl was then added to each microcentrifuge tubes that had either Hist_2 and Hist_23 aptamers, while 0.025 M NaCl was added to microcentrifuge tubes with either Hist_1min, Hist_2min and Hist_23min

aptamers. The total 200 μL mixed solution was vortexed briefly and incubated for 5 minutes. The desired NaCl concentration that is aptamer dependent was determined through a series of salt and aptamer optimization as previously stated. Each sample was then analyzed by UV-Visible spectrometry using a CARY 300 Bio spectrophotometer (Varian, USA). The experiment was performed in triplicates for each histamine aptamer. In each case of histamine aptamer, the relative absorption ratio between 630 nm and 520 nm (A_{630}/A_{520}) was plotted against increasing histamine concentration. Furthermore, using the GraphPad online Software, the limit of detection (LOD) was calculated using the equation below; with the slope and Sy.x (standard error of estimates) calculated from the calibration curve of the relative absorption ratio between 630 nm and 520 nm (A630/A520) plotted against increasing histamine concentrations.

$$LOD = \frac{3.3 \times Sy.x}{Slope} \qquad (1.1)$$

3.8 Preparation of the Colorimetric Assays for Control Studies

Organic compounds tryptophan, indole, and pyrrole were prepared in 1:1 ethanol/water, while histidine and pyridine were prepared in deionized water. An aliquot of final concentration of 1.5 μM histamine, histidine, pyridine, pyrrole, indole, and tryptophan was added to 8 μL of 10 μM stock aptamer and vortexed briefly, followed by a 30 minutes incubation period. This was repeatedly carried out with all histamine aptamers synthesized. The solution was diluted with deionized water, followed by the addition of 50 μL aliquot of 11.77 nM AuNP solution into each mixed solution and vortexed briefly with a 30 minutes incubation period. A final concentration of 0.041 M NaCl was then added to each mixed solution that had either Hist_2 and Hist_23 aptamers, while 0.025 M NaCl was added to mixed solutions with either Hist_1min, Hist_2min and Hist_23min aptamers and vortexed

briefly. Each sample was then analyzed by UV-Visible spectrometry using a CARY 300 Bio spectrophotometer after 5 minutes incubation (Varian, USA). The experiment was performed in triplicates for each histamine aptamer.

3.9 TEM Characterization of Samples

High resolution TEM images of the samples were recorded by drop-casting 10 μL of 1.5 μM histamine target aptamer-AuNP salt induced aggregated solution on a carbon-coated copper grid. Images were recorded on a FEI Tecnai G2 F20 TEM with a Schottky Field Emitter with high maximum beam current (>100 nA) electron source and imaged with a Gatan ORIUS TEM CCD Camera.

3.10 5' Cyanine Dye Aptamer Synthesis for MicroScale Thermophoresis

Cy-5 histamine labelled aptamer sequences Hist_2, Hist_23 and Hist_23min were prepared using standard phosphoramidite chemistry on a Bioautomation MerMade 6 DNA synthesizer (Plano, TX, USA). Oligonucleotides were labelled with fluorescent 5' Cyanine Dye on the 5' end. Aptamers were synthesized in a 3' to 5' direction through a repeating series of organic reactions. Hist_2 and Hist_23 sequences contained identical 3' and 5' primers, and a randomized region. Aptamer Hist_23min sequence only contained randomized region and no primers were present.

The phosphoramidites, dA-CE, Ac-dC-CE, dmf-dG-CE, and dT-CE were obtained from Glen Research (Sterling, VA, USA). They were each dissolved in anhydrous acetonitrile (Glen Research) to create 0.1 μM solutions of each amidite in argon atmosphere. 5' Cyanine Dye was obtained from Glen Research (Sterling, VA, USA). Ultra-High Purity 5.0 argon was purchased from Praxair Canada (Mississauga, ON, Canada). The dissolved phosphoramidites

were connected to the DNA synthesizer along with anhydrous acetonitrile (BDH VWR analytical), activator solution, deblock solution, cap A solution, cap B solution, and oxidizer solution all obtained from Glen Research (Sterling, VA, USA). The 1000 Å 1.0 μmole-controlled pore glass synthesis columns (Biautomation) for each Hist_2 and Hist_23 aptamers contained an initial thymine, while Hist_23min contained an initial cytosine. The columns were also connected to the DNA synthesizer. The appropriate script file was loaded on the MerMade software and synthesis was performed overnight.

Table 3. 2 Cy5 labelled histamine aptamers stored in MST buffer assay used in binding assay experiment.

Sequence Name	**MST Assay Buffer**
Hist_2	10 mM Tris-HCl, 500 mM NaCl, 50 mM $MgCl_2$, 0.005% Tween 20, pH 7.4, 0.005 % Tween20
Hist_23	Same as Hist_2
Hist_23min	Same as Hist_2

3.11 Purification of 5' Cyanine Dye Synthetic Oligonucleotides

Following DNA synthesis, the 4,4'-dimethoxytrityl (DMT) oligonucleotide was deprotected in 1 mL of ammonium hydroxide at 65℃ for 2 hours. Once cooled at room temperature, a 1 mL of 100 mg/mL sodium chloride solution was added to the deprotected DMT-ON oligonucleotide for a final volume of 2 mL. The 150 mg Glen-Pak DNA Purification Cartridges (Glen Research) were conditioned using 0.5 mL of acetonitrile followed by 1 mL of 2 M TEAA on the vacuum pump. The acetonitrile washes organic residues from resin,

while the TEAA acts as an ion-pairing reagent to enhance the binding of the DMT-ON oligonucleotide to the resin. The oligo/salt mixture was applied onto the cartridge in 1 mL aliquots. During the loading process, the DMT-ON oligos are bound to the cartridge, while failure sequences are not retained. The cartridge was then washed with 2 x 1 mL of salt wash solution (5% Acetonitrile in 100 mg/mL Sodium Chloride) to wash away the remainder of the failure sequences from the cartridge. The cartridge was then washed with 2 x 1 mL of deionized water, rinsing away the excess salts. The purified oligos were eluted into sample tubes using 1 x 1 mL 50% acetonitrile in water with 0.5% ammonium hydroxide. The collected oligos were dried down by a SpeedVac overnight, an Automatic Environmental SpeedVac® System AES2010 (Savant).

3.12 PAGE Purification of 5' Cyanine Dye Synthetic Oligonucleotides

A 18% polyacrylamide/urea gel (63 g of Urea, 47 mL of Acrylamide stock, 30 mL of 5X TBE, 28 mL H_2O) was prepared. The solution was stirred on a hot plate at 37℃. The solution was filtered by gravity and allowed to cool at room temperature. A solution of 10% ammonium persulfate was prepared with 0.45 mL added to the acrylamide solution. A 60 µL of TEMED was quickly added to the solution and mixed thoroughly. The plates were filled with the solution and appropriate combs were inserted. The acrylamide was allowed to polymerize for 30 minutes. The combs were then removed, and the loading area was rinsed with deionized water. The plates were placed into the gel system with the electrode wires attached. The bottom gel system was filled with 1X TBE about 1 inch above the bottom of the gel. The top was also filled with 1X TBE to cover the electrode wire. The system ran without the samples for 15 minutes at 75 V. The DNA samples were then prepared by adding 200 µL of deionized water and vortexed briefly. An equal amount of formamide was

added to the DNA samples and vortexed briefly. The DNA sample solutions were then heated to 90℃ for 5 mins. The system ran for a further 2 hours at 250 V.

The bands on the gel were visualized on the Alpha Imager (AlphaEaseFC). The bands were cut out and placed in 15 mL Eppendorf tubes. Deionized water was added, and the tubes were shaken to break up the gel. The tubes were allowed to incubate at 37℃ for at least 24 hours at 120 rpm in the shaker/warmer (Innova 40 by New Brunswick Scientific). The gel slurry was filtered with a 10 mL syringe attached to a PEG filter (0.22 μm, 30 mm diameter) in a 50 mL Eppendorf tube. The lid tubes were poked holes using needles, and the tubes containing the filtered gels were frozen with liquid nitrogen and placed on the lyophilizer (LABCONCO FreeZone[4.5]).

The samples were removed from the lyophilizer and were dissolved in deionized water. Desalting tubes were prepared per sample. The de-salting tubes were washed with water and centrifuged at 14000 rpm for 20 mins (Sorvall Legend Micro Centrifuge, Thermo Electron Corporation). The flow-through was then discarded and 500 μL of sample was added to the desalting tubes and centrifuged at 14000 rpm for 20 mins. Once all sample passed through the filter, the de-salting tubes were washed 4x with 500 μL of deionized water. The DNA samples were collected by inverting the de-salting filters upside down into a clean de-salting tube and centrifuged at 4000 rpm for 5 mins. The samples were collected and placed on Speed Vac.

3.13 Quantification of 5' Cyanine Dye Aptamers using UV-Vis Spectroscopy

Synthesized DNA concentration was determined using UV-Vis spectroscopy; a CARY 300 Bio spectrophotometer (Varian, USA). Aliquots of the DNA stock solutions were diluted with deionized water, in order to measure absorbances between 0.4-0.8 at 256 nm. The Beer-

Lambert Law equation was used to determine the concentration of each aptamer using the measured absorbance value and the theoretical extinction coefficient, provided through the use of OligoAnalyzer® Tool, version 3.1, on the Integrated DNA Technologies (IDT) website (PrimerQuest® program, IDT, Coralville, Iowa, USA). The aptamers were diluted and stored in 10 mM Tris-HCl, 50 mM $MgCl_2$, 0.5 M NaCl, pH 7.4 buffer at -20°C as indicated in **Table 3.2**.

The purity of the aptamer was determined through molecular weight verification by mass spectrometry. Samples of 1 nmol of the aptamer solution were dried using the SpeedVac and sent to Novatia for electrospray ionization (ESI) mass spectrometry analysis.

3.14 Preparation for MicroScale Thermophoresis (MST)

Samples were prepared for MST experiment. Cy5 labelled aptamers Hist_2, Hist_23, and H_23min were each diluted in Tris-HCl buffer to make a final 50 µL of 10 µM stock. Target histamine as well as histidine were each diluted in Tris-HCl buffer to make a final 50 µL of 500 µM stock. The samples were shipped in dry ice to 2bind GmbH (Regensburg, Germany) where the experiment was performed.

A serial dilution of the ligand was prepared in a way to match the final buffer conditions in the reaction mixture (assay buffer: 10 mM Tris-HCl, 50 mM $MgCl_2$, 0.5 M NaCl, pH 7.4, 0.005 % Tween20). The highest concentration of ligand was 100 µM and the lowest 3.05 nM. A 5 µL of each dilution step were mixed with 5 µl of the fluorescent aptamer. The final reaction mixture, which was filled in capillaries, contained a respective amount of ligand (maximum concentration 50.0 µM, minimum concentration 1.53 nM) and constant 200 nM fluorescent aptamer. The samples were analyzed on a Monolith NT.115 at 25°C, with 65% LED power and 40% Laser power.

Chapter 4: Results and Discussion

4.1 DNA Synthesis Quantification

The Beer-Lambert Law equation was used to determine the concentration of each aptamer using the measured absorbance value at λmax=256 and the theoretical extinction coefficient. **Table 4.1** shows the calculated concentrations of each synthesized aptamer. All DNA concentrations were diluted to make the final 10 μM stock solutions that were used in the colorimetric assay experiment.

Table 4. 1 DNA quantification by UV/Vis at λmax=256 using a CARY 300 Bio spectrophotometer (Varian, USA)

Aptamer	Absorbance	Extinction Coefficient (L/mol·cm)	Concentration (mol/L) (10^{-6})	Concentration × DF (mol/L) (10^{-3})	nmol	Molecular Weight (g/mol)
Hist_1min	0.551	392500	1.410	1.050	210.6	12519.1
Hist_2min	0.617	401700	1.530	1.150	368.6	12639.2
Hist_23min	0.541	392300	1.370	2.060	413.7	12581.1
Hist_2	0.499	705500	0.707	0.707	212.2	22342.4
Hist_23	0.362	696400	0.520	0.520	155.9	22284.4

DNA synthesis was confirmed through molecular weight verification using electrospray ionization (ESI) mass spectrometry. As illustrated in **Figure 6.1 Appendix A**, the molecular ion peak obtained in all five aptamers were confirmed as indicated in **Table 4.1**. Overall, these mass spectrum results demonstrated that the DNA synthesis was complete.

4.2 Secondary Structure Prediction of Aptamers

Potential G-quadruplex structures were analyzed in all aptamers using the QGRS (Quadruplex forming G-Rich Sequences) Mapper software. G-rich aptamers have the ability to fold into stable G-quadruplex structures under physiological conditions and recognize different targets [67,68]. G-quadruplex structures are stacking interactions of G-quartets, in which they are an association of four guanine molecules connected through Hoogsteen hydrogen bonds that forms a square planar complex as shown in **Figure 4.2.1**. The G-quartets are stabilized by cations centrally coordinated to the oxygen molecules of the guanines [67]. G-rich aptamers have shown to be more thermodynamically and chemically stable compared to unstructured sequences. The highly localized negatively charged G-quadruplex structures also provides strong electrostatic binding to the positively charged surfaces of targets [67,68]. It was determined that all histamine aptamers have possible G-quadruplex formation as shown in **Table 4.2**, potentially contributing to the aptamers thermodynamic and chemical stability.

Furthermore, the secondary structures of the aptamers were predicted using RNAstructure[90] online software tool. **Figure 4.2.2** displays the determined minimum free energy structures of the aptamer sequences. Potential secondary structures of aptamers can model the binding regions of aptamers. In all aptamers, stem loops were observed showing potential binding sites towards the target histamine.

Moreover, as displayed in **Figure 4.2.2**, Hist_2min and Hist_23min have similar predicted secondary structures, indicating a likelihood that these two sequences are in the same sequence family. Using the Standard Nucleotide BLAST® online software, these aptamers were analyzed to determine if they are likely from the same sequence family. A BLAST Score

of 52.8 % was observed, indicating that there is a possibility that Hist_2min and Hist_23min aptamers are derived from the same sequence family.

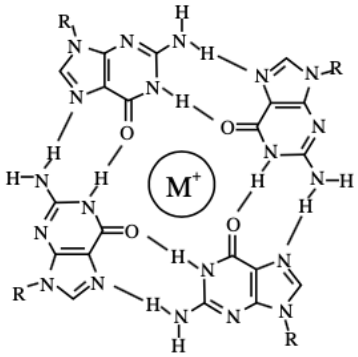

Figure 4.2. 1 Schematic representation of a G-tetrad stabilized by a metal ion in the central cavity [69][67]

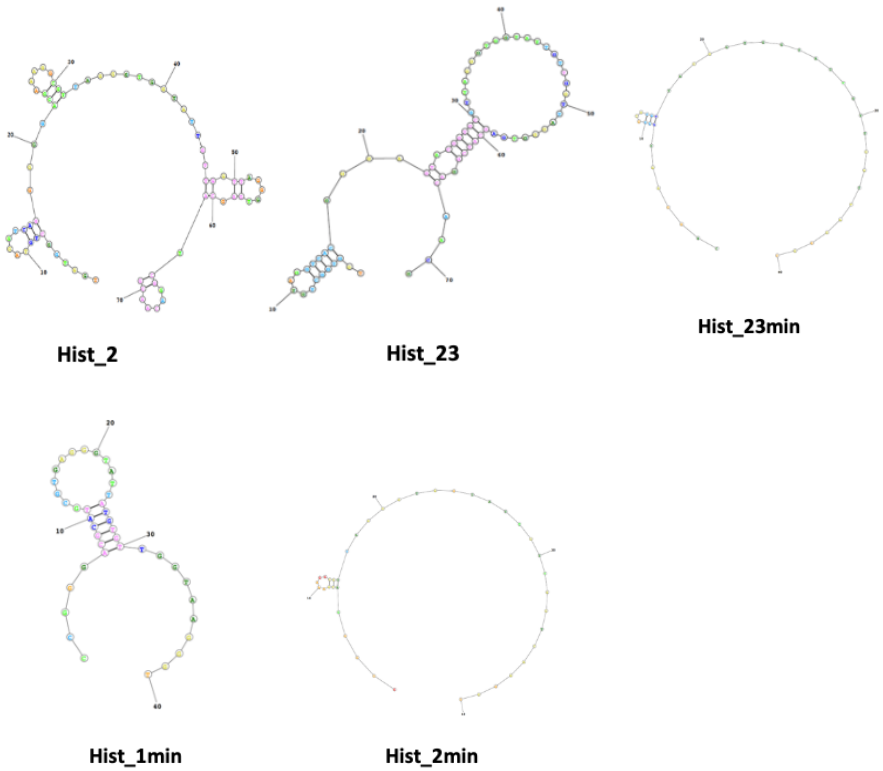

Figure 4.2. 2 Minimum free energy conformations of the predicted secondary structures of Hist_1min, Hist_2min, Hist_23min, Hist_2, and Hist_23 aptamers.

Table 4. 2 Predicted mapping of G-quadruplex elements in Hist_1min, Hist_2min, Hist_23min, Hist_2, and Hist_23 aptamers. The G-score of each aptamer was generated by the QGRS Mapper.

Aptamer	**Length (bases)**	**G-Score**
Hist_1min	40	28
Hist_2min	40	34
Hist_23min	40	32
Hist_2	71	68
Hist_23	71	68

4.3 AuNP Synthesis

Synthesized AuNPs were quantified by UV-Vis spectrometry, displaying a λmax =520 nm as displayed in **Figure 4.3.1**. At a dilution factor of 1:10, the stock concentration calculated was 11.77 nM. The synthesized AuNPs were also visualized by HR TEM to determine their average sizes as shown in **Figure 4.3.2**. The AuNPs displayed an average size of around 14.3 nm.

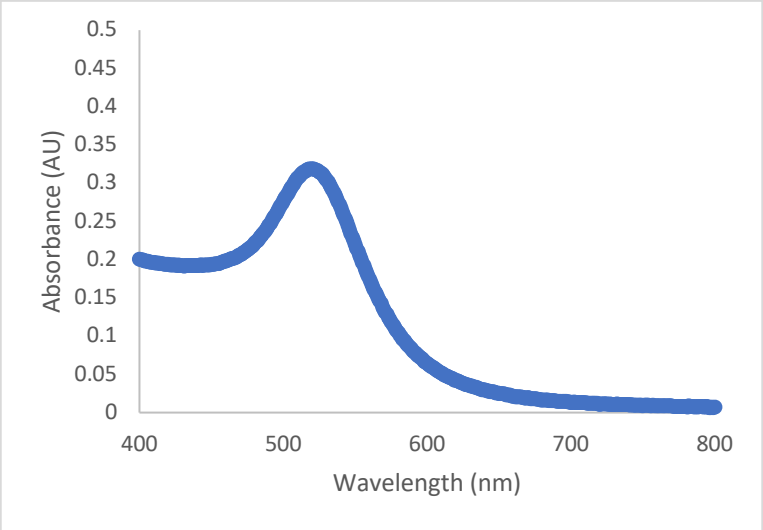

Figure 4.3. 1 UV-Vis spectrometry of synthesized AuNPs, displaying a λmax =520 nm with the calculated concentration determined to be 11.77 nM using a CARY 300 Bio spectrophotometer (Varian, USA).

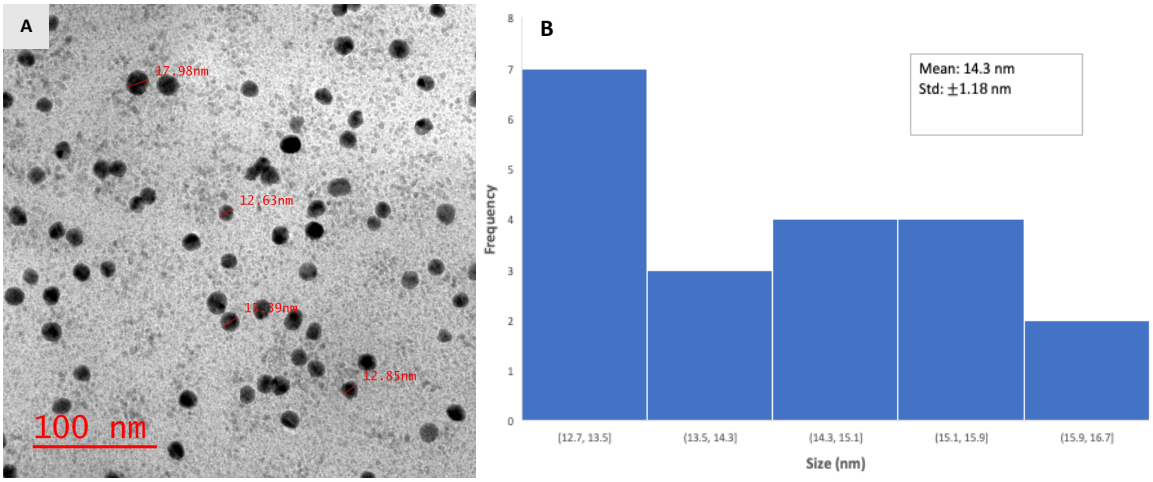

Figure 4.3. 2 (A) HR TEM image displaying size distribution of AuNPs using FEI Tecnai G2 F20 TEM, **(B)** and corresponding histogram

4.4 Colorimetric Assay Salt Optimization

A series of salt optimizations were conducted in order to determine the concentration of NaCl required to induce AuNP aggregation. The negatively charged citrate-coated surfaces of AuNPs enables them to be stable in aqueous solution. As salt is present in the AuNP solution, the high ionic strength hinders the stability of AuNPs by decreasing the screening length of the negatively charged citrate capping agents on the nanoparticle surfaces. This

leads to an increase in van der Waals interaction between nanoparticles that results to AuNP aggregation and sedimentation. Both the cations and anions of the salt affect the stability of AuNPs by various mechanisms [70]. The cations increase the ionic strength and screen the negative charges on AuNPs to cause aggregation. Anions may also adsorb on AuNPs and exert stabilization effect; however, it has recently been studied that they may also displace adsorbed DNA or inhibit DNA adsorption (e.g. Br-, I-), leading to the loss of protection by the DNA and decreased colloidal stability [70,71].

In this experiment, salt optimization was carried out using 0.25 M and 0.33 M stock solutions of NaCl. Salt induced AuNP aggregation was carried out with the mixture of diluted AuNP solutions with increasing concentrations of NaCl as shown in **Figure 4.4.1**. It was determined that a concentration range between 0.025-0.041 M of NaCl induced AuNP aggregation. This NaCl concentration range was utilized for further DNA and target histamine optimizations, until an ideal salt concentration was determined for final colorimetric studies. It is important to determine the optimal concentration of NaCl needed for the assay. If the concentration of NaCl is too low, the aggregation of AuNPs will not be induced as observed in the figure below. On the contrary, a high concentration of NaCl can disturb the stability of the AuNPs-aptamer conjugates and hinder the sensitivity of the assay [63].

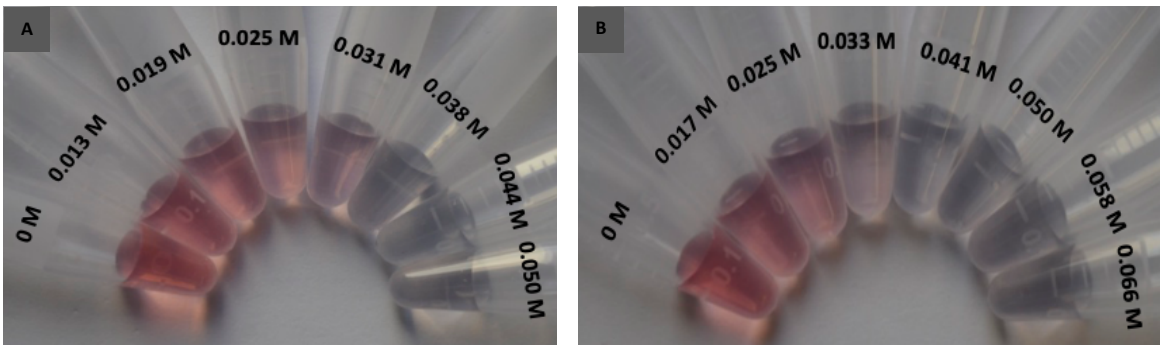

Figure 4.4. 1 Photograph of the mixture of diluted AuNP solutions with increasing concentration of **(A)** 0.25 M, **(B)** 0.33 M Stock NaCl

4.5 Colorimetric Assay DNA Optimization

A series of DNA optimizations were carried out in order to obtain the ideal aptamer concentration for the colorimetric study. Initially, as demonstrated in **Figure 4.5.1-4.5.5 (A)**, aptamer-AuNP control assays were carried out for all five aptamers Hist_1min, Hist_2min, Hist_23min, Hist_2 and Hist_23, respectively. These control assays were carried out to determine whether any of the histamine aptamers incubated with diluted AuNP solutions triggered AuNP aggregation. The results showed no evidence of AuNP aggregation as a result of DNA interaction, therefore removing false positives.

Further DNA optimization studies were conducted to determine the ideal aptamer concentration that can effectively stabilize AuNPs against salt-induced aggregation. As aptamers are incubated in AuNP solution, the aptamers are adsorbed onto the surface of AuNPs stabilizing them against salt-induced aggregation [54,70]. There are two types of interaction that occurs between ssDNA and AuNPs. Exposed bases in aptamers are adsorbed onto AuNPs, with adenine having the highest adsorption affinity, while thymine has the lowest affinity among the four bases [54,72]. However, there are also electrostatic repulsion between the negatively charged phosphate backbone and the negatively charged AuNPs. This electrostatic repulsion is highly frequent in folded ssDNA (e.g., G-quadruplexes) [54]. Overall, there is a stronger interaction between the bases of aptamers and AuNPs than electrostatic repulsion between the negatively charged phosphate backbone and the negatively charged AuNPs [53].

As the concentration of aptamer is increased, a decline of salt-induced AuNP aggregation is observed as shown in **Figure 4.5.1-4.5.5 (B)**. The optimal aptamer concentration chosen for the colorimetric histamine target assay, is at which there is an absence of salt induced AuNP aggregation observed. The ratio between the AuNPs and aptamer is important and

could affect the final sensitivity of the assay. Excess amount of aptamers in the solution could reduce the sensitivity of the sensor by not achieving a lower limit of detection, while very little amount of aptamers could decreases the stability of the AuNPs [53,63]. After a series of multiple trials, a final concentration of 0.40 μM of DNA for all aptamers, was chosen as the optimal DNA concentration to be used for further colorimetric histamine target assay.

Furthermore, it was observed that Hist_1min, Hist_2min, and Hist_23min aptamer-AuNP-salt solutions, exhibited lower stability compared to the other Hist_2 and Hist_23 aptamer-AuNP-salt solutions. One theory could be the effect of aptamer length on salt induced AuNP aggregation. Hist_1min, Hist_2min, and Hist_23min are all 40 bases long, while Hist_2 and Hist_23 aptamers are 71 bases long, respectively. One can discuss the possibility that the full-length aptamers have more bases that strongly interacts with the AuNP surfaces, stabilizing the AuNPs in the presence of salt, compared to the truncated minimers that have fewer bases. Studies have shown that longer ssDNA have a better stabilization effect than shorter ssDNA at the same molar concentration, due to longer ssDNA having more bases [53]. To minimize the aggregation occurring in Hist_1min, Hist_2min, and Hist_23min aptamer-AuNP salt solutions, the concentration of NaCl was reduced. After a series of salt optimizations, 0.025 M of NaCl was used for further colorimetric assays in regards with Hist_1min, Hist_2min, and Hist_23min aptamers; while 0.041 M of NaCl was used in regards with Hist_2 and Hist_23 aptamers.

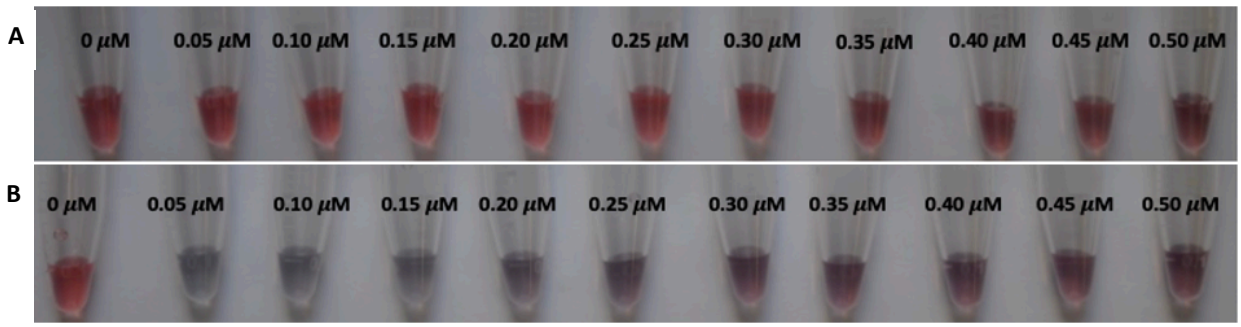

Figure 4.5. 1 Photograph of **(A)** mixture of diluted AuNP solutions with increasing concentration of Hist_1min (10 μM stock) **(B)** mixture of diluted AuNP solutions with increasing concentration of Hist_1min (10 μM stock), in the presence of 0.041 M of NaCl.

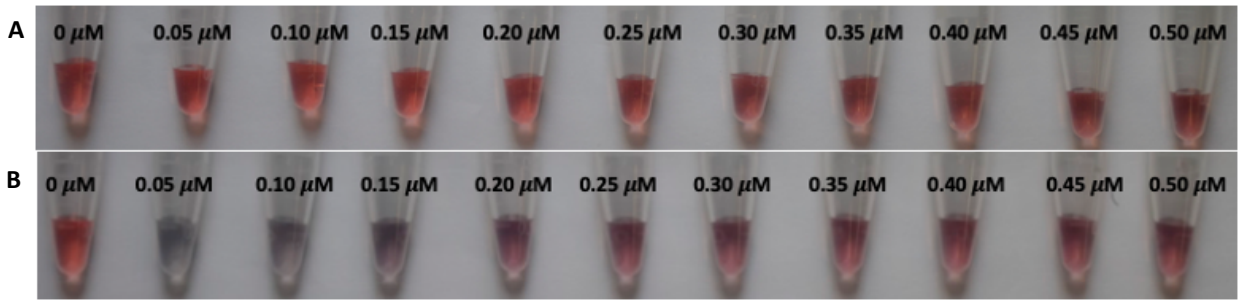

Figure 4.5. 2 Photograph of **(A)** mixture of diluted AuNP solutions with increasing concentration of Hist_2min (10 μM stock) **(B)** mixture of diluted AuNP solutions with increasing concentration of Hist_2min (10 μM stock) in the presence of 0.041 M of NaCl.

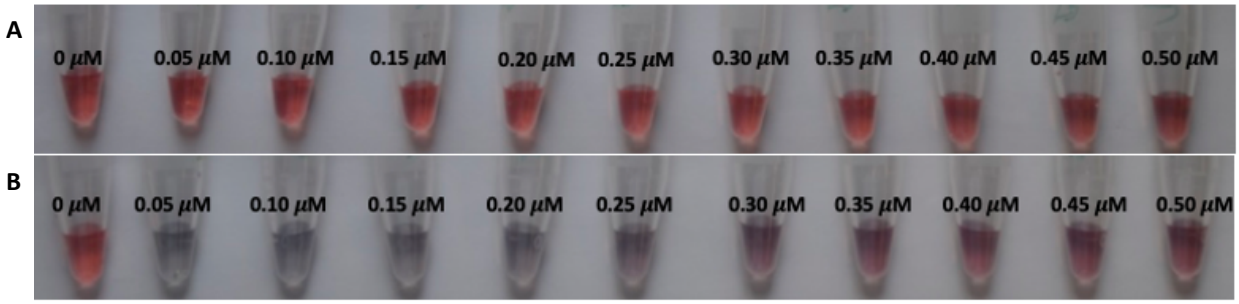

Figure 4.5. 3 Photograph of **(A)** mixture of diluted AuNP solutions with increasing concentration of Hist_23min (10 μM stock) **(B)** mixture of diluted AuNP solutions with increasing concentration of Hist_23min (10 μM stock) in the presence of 0.041 M of NaCl.

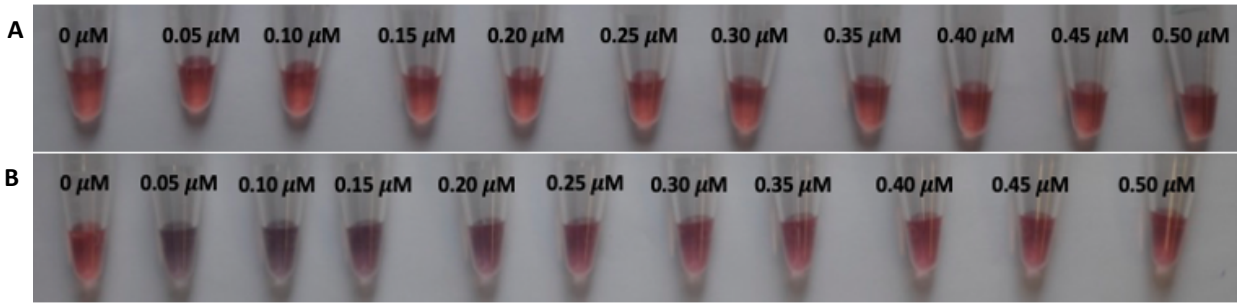

Figure 4.5. 4 Photograph of **(A)** mixture of diluted AuNP solutions with increasing concentration of Hist_2 (10 µM stock) **(B)** mixture of diluted AuNP solutions with increasing concentration of Hist_2 (10 µM stock) in the presence of 0.041 M of NaCl.

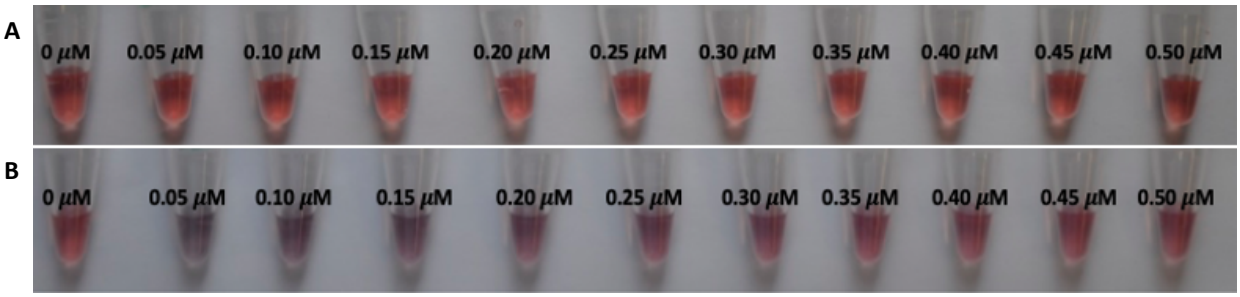

Figure 4.5. 5 Photograph of **(A)** mixture of diluted AuNP solutions with increasing concentration of Hist_23 (10 µM stock) **(B)** mixture of diluted AuNP solutions with increasing concentration of Hist_23 (10 µM stock) in the presence of 0.041 M of NaCl.

4.6 Colorimetric Assay for Histamine Control Experiment

It is critical to design control experiments to determine any potential factors that might influence the mechanism of the assay. A control experiment was conducted to determine whether or not target histamine molecule itself triggers AuNP aggregation, that may result in false positive in the experiment. It is important that the target does not interact with AuNP surfaces, as this may hinder the stability of AuNPs [53,72]. To make sure no false positives occurred, increasing concentration of histamine was incubated in AuNP solution for 30 minutes. Absence of AuNP aggregation was observed in the presence of increasing concentration of target histamine as shown in **Figure 4.6.1**. This eliminates any false positives throughout the colorimetric assay experiment, when target histamine is present. Other factors that could affect the mechanism of the assay, includes the use of buffers, as

the medium could also interact with AuNP surfaces, displacing the adsorbed DNA [71,72]. However, this assay was solely conducted in water solution and no buffer was used, hence eliminating another potential source that might give false positives and even affect the sensitivity of the assay.

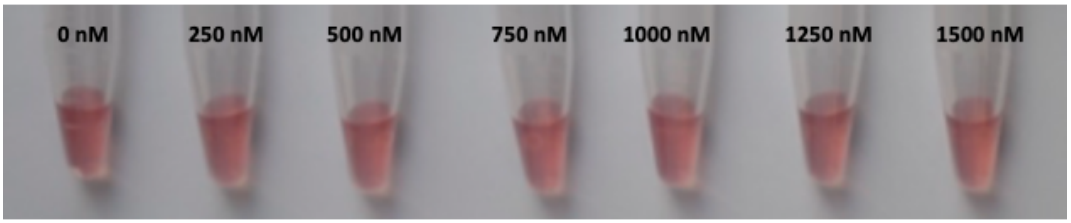

Figure 4.6. 1 Photograph of the mixture of AuNP solutions with increasing concentration of histamine (0-1500 nM).

4.7 Colorimetric Assay for the Detection of Histamine

Characterization of histamine aptamers was conducted through in-solution colorimetric assay, to determine the binding affinity and specificity of the histamine aptamers. This characterization technique is simple, rapid and can be visualized with naked eyes. In this study a "reverse adsorption-desorption" colorimetric approach was adopted, whereby aptamers were initially incubated with target histamine, followed by the incubation of mixed solution with AuNPs. In the presence of histamine, aptamers preferably bind specifically onto target, releasing AuNPs to aggregate upon addition of salt. In the absence of target histamine, all aptamers exhibited a red color AuNPs-salt solution as shown in **Figure 4.7.1**. This is due to the aptamers being adsorbed onto the surfaces of AuNPs, hindering the ability of salt to neutralize the stabilizing citrate negative charges around the surface of AuNPs, allowing the AuNPs to remain dispersed. As the concentration of histamine target increases the AuNPs aggregate and exhibit a purple-blue color, as shown in

Figure 4.7.1. In the presence of target, histamine aptamers preferably bind to histamine, releasing AuNPs to aggregate upon salt addition. As observed in **Figure 4.7.1**, all histamine aptamers exhibited AuNP aggregation at histamine concentrations of 500 nM to 1500 nM, with color changing from red to purple-blue. It is important to note that aptamer Hist_1min-AuNP-salt solution continued to show some aggregation in the absence of target, even after multiple salt optimizations. Therefore, in comparison to other aptamer-AuNP solutions, aptamer Hist_1min-AuNP salt solutions showed more aggregation as the concentration of target increased. This could potentially affect the reliability of the Hist_1min aptamer colorimetric assay study.

Furthermore, the colorimetric assay for the detection of histamine was quantified and analyzed by UV-Vis spectrometry. In the absence of target histamine, the AuNPs remain dispersed and exhibit a red color with a strong absorption band at 520 nm attributed to the localized SPR. As the histamine target concentration increases, AuNPs aggregate in the presence of salt leading to a color change from red to blue. As the distance between the nanoparticles decrease, near-field coupling starts to occur, resulting in a red shift in the absorption band to 630 nm. The new absorbance maximum is highly dependent on the distance between nanoparticles. Consequently, as observed in **Figure 4.7.2**, the intensity of absorption band at 520 nm decreases, while the peak at 630 nm increases as the concentration of histamine increases. This pattern is observed in all histamine aptamers. However, there were differences in 630 nm peak intensity observed between aptamers, with some aptamers showing stronger 630 nm peak intensity compared to others. Moreover, some aptamers exhibited the 630 nm peak at a lower concentration of histamine target compared to other aptamers. The bathochromic shift in the plasmon with an increase in 630nm peak intensity corresponds to the visual color change of AuNP aggregation

observed in **Figure 4.7.1**. These results demonstrate that all the aptamers have strong binding affinity towards target, with some aptamers exhibiting stronger binding compared to other aptamers.

To determine the binding affinities of each aptamer, a calibration curve of the colorimetric assay of each aptamer was set up. The ratio of the absorbance at 630 nm to the absorbance at 520 nm (A_{630}/A_{520}) was plotted as the function of increasing histamine concentrations in all aptamer-AuNP solutions as illustrated in **Figure 4.7.3**. Overall, all aptamers showed good linearity with most of them exhibiting linearity as low as 100 nM concentration of histamine target. Using the calibration curves, the limit of detections (LOD) of each aptamer was calculated. As tabulated in **Table 4.3**, Hist_23min and Hist_2 showed lowest LOD values at 300 nM and 400 nM respectively, demonstrating that they have stronger binding affinity compared to other aptamers. Aptamer Hist_2min showed the highest LOD value at 800 nM histamine concentration.

One can potentially improve the sensitivity of the assay in various ways for further studies. The sensitivity of the assay is dependent on the molar extinction coefficient of the AuNPs, which is dependent on the particle size. The use of larger AuNP nanoparticles (30-50 nm) have shown to offer higher sensitivity due to their higher molar extinction coefficients [54,61]. The plasmonic coupling of large AuNPs gives higher magnitude peak shift when aggregation occurs compared to small AuNPs. Interestingly, normally the larger nanoparticles diffuse slower and may give a slower aggregation rate. However, the high peak shift of large AuNPs suggests a dominant contribution of the plasmonic coupling strength over aggregation rate [61]. By further studying these AuNP design parameters, one could potentially improve the sensitivity of the assay.

Additionally, the sensitivity of the assay could be improved by altering the methodology of the experiment. Conventionally, NaCl has been the most commonly used salt to induce aggregation. However, chloride ions are shown to have stronger affinity towards AuNP surfaces than fluoride ions, potentially displacing some weakly adsorbed DNA [70,72]. Therefore, NaF could potentially be an improved alternative salt medium, increasing the sensitivity of the assay [70]. Further research should be conducted on this topic, but this could potentially improve the sensitivity of the colorimetric assay performed in this study. Furthermore, one could utilize amino modified positively charged AuNPs as an alternative for the negatively charged AuNPs. This mechanism does not require salt to induce aggregation, therefore removing any effect of salt medium that might lower the sensitivity of the assay. The use of positively charged AuNPs have proved to improve the sensitivity of the assay, as the interaction between the aptamer and target cannot be affected by the salt concentration [42]. Moreover, the methodology could also be altered by adding a centrifugation and resuspension approach to the aptamer-AuNP-target solution that could potentially improve the sensitivity of the assay. In a recent study, it has shown that this approach forces the complete dissociation of aptamers that are still adsorbed onto the AuNPs surface after target recognition. Residual aptamers that remain to be adsorbed onto the AuNPs surface inspite of target addition, greatly hinders the sensitivity of the sensor by preventing the nanoparticles from aggregating when the optimized salt concentration is added [43]. However, this proposed methodology could affect the equilibrium that is established, potentially influencing the aptamer-target interaction. Further research on this methodology approach is recommended.

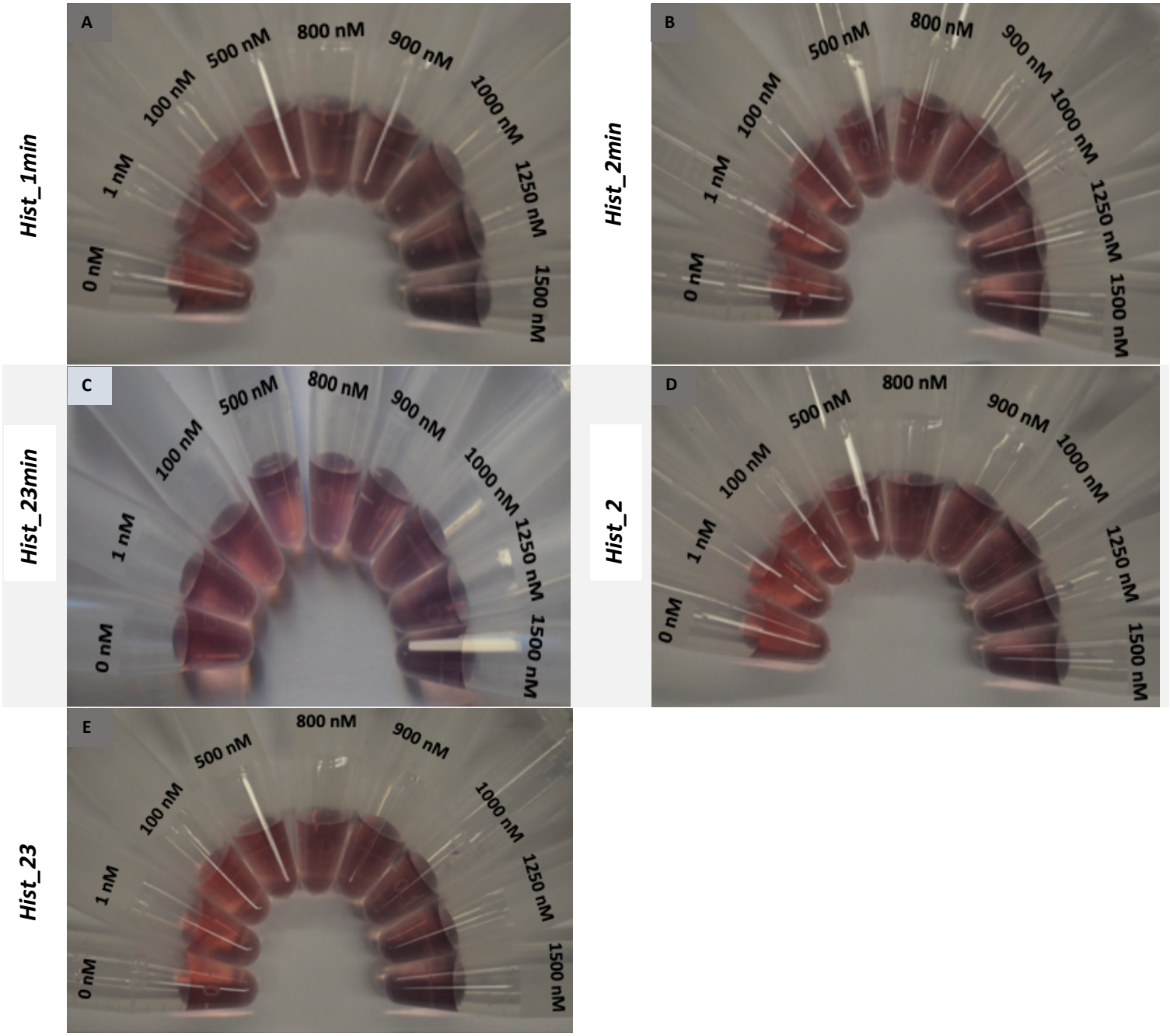

Figure 4.7. 1 Photographs of the mixture of **(A)** Hist_1min-AuNPs, **(B)** Hist_2min-AuNPs, **(C)**, Hist_23min-AuNPs, (**D)** Hist_2-AuNPs, **(E)** Hist_23-AuNPs solutions in the presence of increasing concentration of histamine (0-1500 nM).

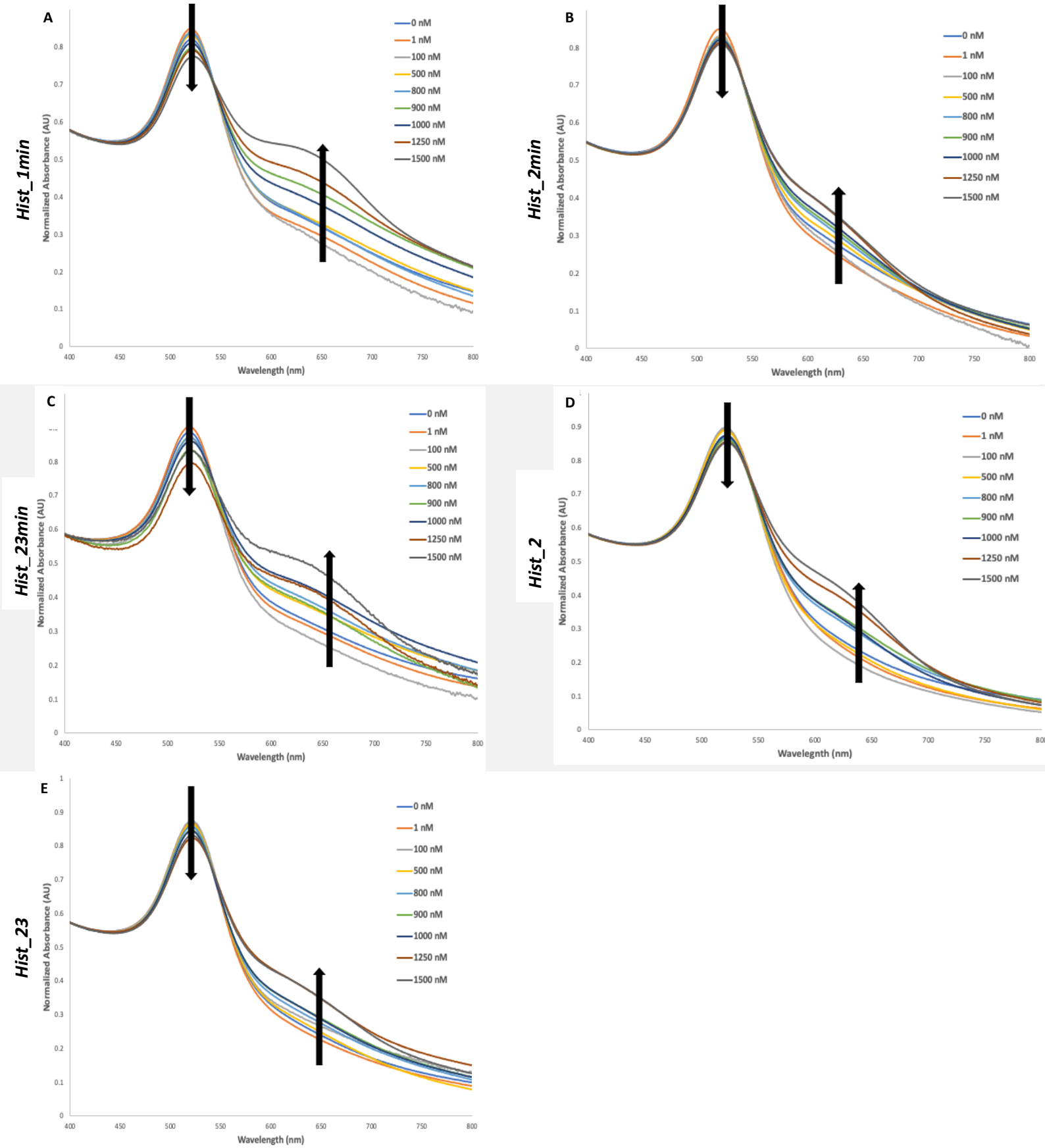

Figure 4.7. 2 Spectral changes from the assembly of **(A)** Hist_1min-AuNP, **(B)** Hist_2min-AuNP, **(C)** Hist_23min-AuNP, **(D)** Hist_2-AuNP, **(E)** Hist_23-AuNP in deionised water, upon the addition of increasing concentration of histamine (0-1500 nM).

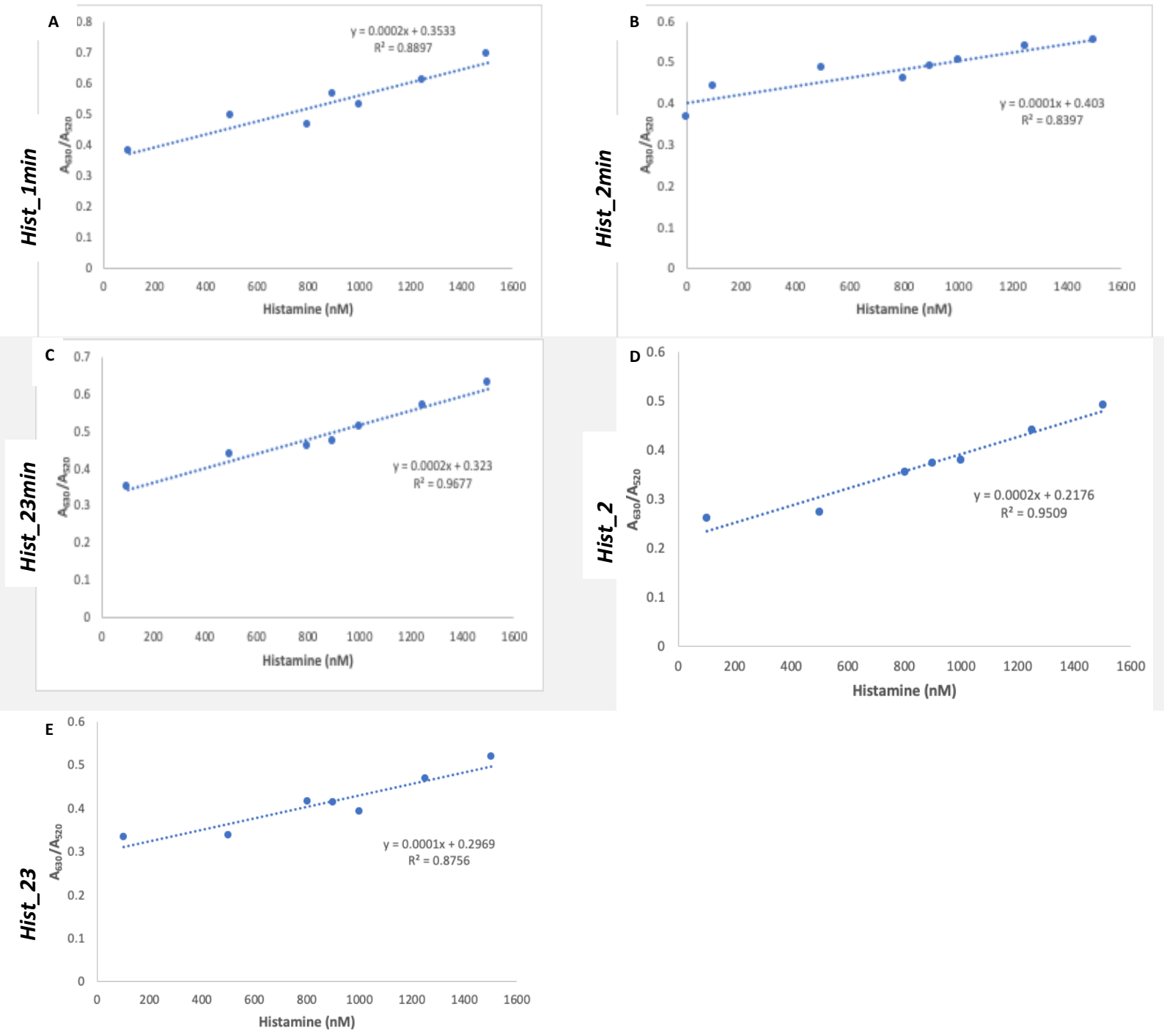

Figure 4.7. 3 Calibration curve for the colorimetric assay; ratio of the absorbance at 630 nm to the absorbance at 520 nm (A_{630}/A_{520}) plotted as the function of increasing histamine concentration in **(A)** Hist_1min-AuNP, **(B)** Hist_2min-AuNP, **(C)** Hist_23min-AuNP, **(D)** Hist_2-AuNP, **(E)** Hist_23-AuNP solutions.

Table 4. 3 Calculated LODs for histamine aptamers

Aptamer	**LOD (nM)**
Hist_1min	600
Hist_2min	800
Hist_23min	300
Hist_2	400
Hist_23	600

4.8 TEM Analysis

In this study, the mechanism of salt induced aptamer-AuNP aggregation in the presence of target histamine was supported by TEM analysis. As observed in **Fig 4.8.1**, in the absence of histamine target, aptamer-AuNPs are well dispersed and uniform in aqueous salt solution. All the aptamers studied showed similar observations. As the aptamer-AuNPs are incubated in 1.5 μM histamine target, the AuNPs aggregate in the presence of salt as observed in **Fig 4.8.1** below. High resolution TEM studies, has supported the proposed colorimetric assay mechanism, confirming all the histamine aptamers showed binding affinity towards target histamine.

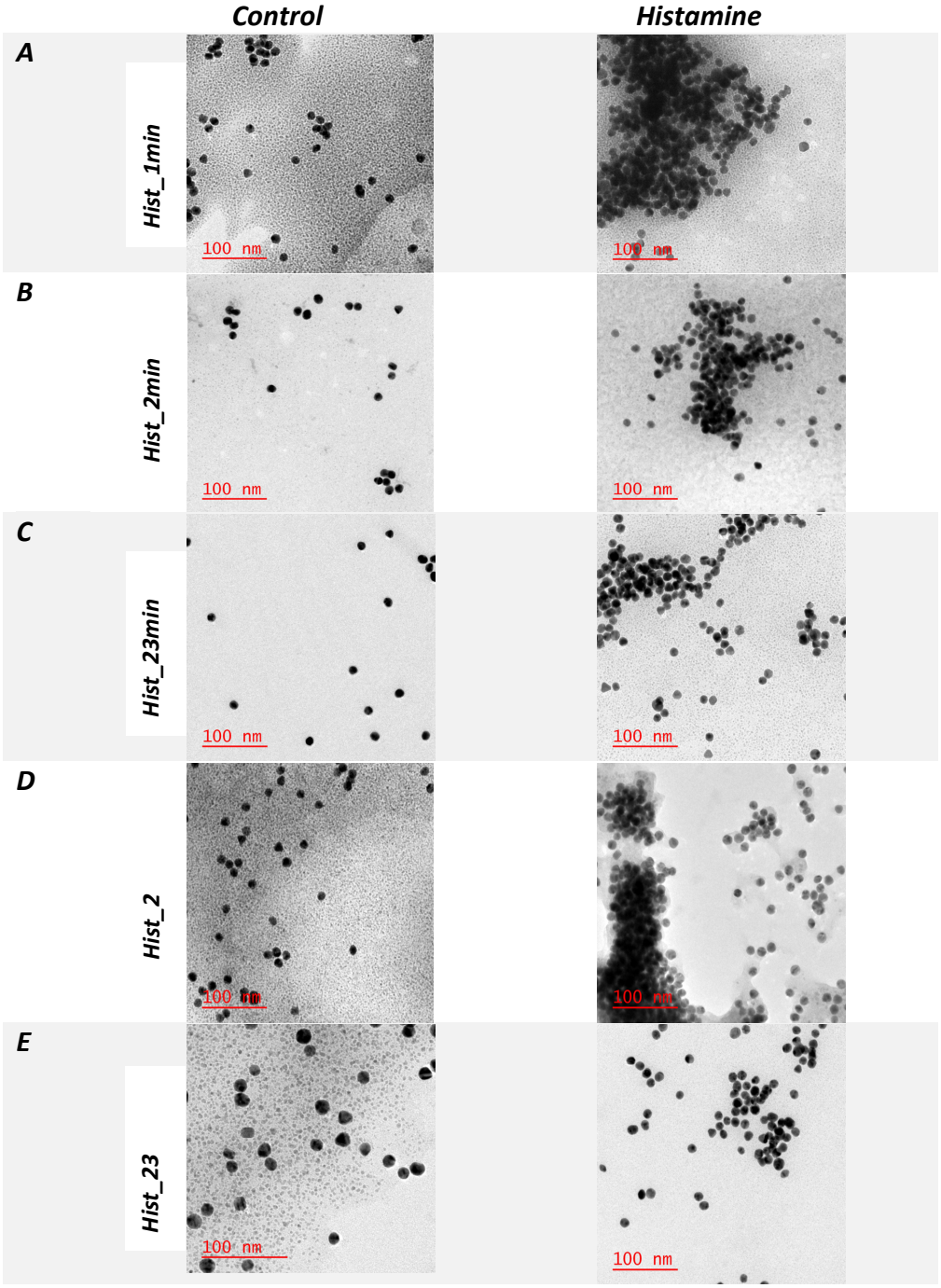

Figure 4.8. 1 HR TEM images of **(A)** Hist_1min-AuNPs, **(B)** Hist_2min-AuNPs, **(C)** Hist_23min-AuNPs, **(D)** Hist_2-AuNPs, **(E)** Hist_23-AuNPs in the absence of target histamine (left) and with 30 minutes incubation in the presence of 1.5 µM histamine target (right).

4.9. Colorimetric Assay for Control Studies

In this experiment, the binding specificity of the selected histamine aptamers were studied to determine any cross-reactivity with other structurally similar organic compounds. Structurally, the histamine target comprises of an imidazole ring and an aliphatic amino group connected by a two-carbon chain atom. The amino and imidazole groups are both basic, and under physiological conditions (pH 7) histamine is mainly protonated at the aliphatic amino group [3]. Organic compounds that exhibit similar structures to histamine target were obtained, and control experiments were conducted to determine the binding specificity of the selected histamine aptamers. The organic compounds selected were histidine, indole, tryptophan, pyrrole, and pyridine. These organic compounds contained nitrogen ring structures, with some possessing an imidazole ring and an aliphatic amino group as observed in **Table 4.4**. Colorimetric assay experiments were performed in the presence of each organic compound including histamine target. As observed in **Figure 4.9.1**, all aptamers exhibited some AuNP aggregation in the presence of histidine, a histamine precursor, while there was little to no AuNP aggregation observed in other control organic compounds with most aptamers. Aptamer Hist_1min seemed to show significant aggregation in the presence of other organic compounds. However, as stated earlier aptamer Hist_1min-AuNP solution continued to show some aggregation in the absence of either target or other control organic compounds, hence making it difficult to predict the reliability of the results presented.

Furthermore, these control colorimetric assay studies were analyzed by UV-Vis spectroscopy as shown in **Figure 4.9.2**. In the presence of target histamine, there was a clear absorption peak at 630 nm and a reduced peak intensity at 520 nm, explicitly indicating the occurrence of AuNP aggregation. In the presence of histidine organic

compound, an absorption peak at 630 nm was also observed in all aptamer-AuNP solutions, confirming the occurrence of AuNP aggregation. This is potentially due to structural similarities between histamine target and histidine, with both compounds possessing an imidazole ring and an aliphatic amino group as shown in **Table 4.4**. It is also believed that histamine is mainly protonated at the aliphatic amino group in physiological conditions, contributing to the specific binding of histamine aptamers which could probably be the same case as in histidine. These factors potentially contribute to the aptamers slight binding onto histidine. However, there is a significant peak intensity differences between solutions incubated in histamine and that in histidine, revealing that histamine aptamers preferably bind to histamine target compared to histidine. This is probably due to the differing histidine carboxyl group, which is deprotonated under physiological conditions. Moreover, most aptamers showed minimum peak intensity at 630 nm in the presence of other organic compounds (indole, tryptophan, pyrrole, and pyridine) revealing that there is no significant AuNP aggregation occurring. This control study demonstrated the specificity of all the selected histamine aptamers, which is important to determine their reliability in biosensor assays.

In terms of narrowing down and selecting the appropriate aptamers for further binding studies, factors such as aptamers' binding affinity and specificity were considered. Firstly, aptamers were initially narrowed down by their calculated LODs. Aptamers Hist_2, Hist_23, and Hist_23min were selected due to their lowest LODs, indicating their high affinity towards target histamine. Furthermore, aptamers Hist_2, Hist_23, and Hist_23min were also selected due to their specificity towards target histamine. The selected aptamers showed little to no AuNP aggregation in the presence of other organic compounds. Aptamer Hist_1min showed a promising LOD of 600 nM, however there was some significant non-

specific interaction that was observed. In addition, as stated earlier, it was difficult to predict the reliability of the aptamer Hist_1min colorimetric assay results, due to the aptamer Hist_1min-AuNP salt solution aggregating in the absence of either target or other control organic compounds. Therefore, Hist_1min aptamer was not selected for further binding studies.

In conclusion, the colorimetric assay characterization method has determined the binding affinity and specificity of the histamine aptamers. Moreover, three aptamers (Hist_2, Hist_23, and Hist_23min) out of the five aptamers were selected for further binding characterization studies. These histamine aptamers displayed high affinity and specificity towards histamine target, which is ideal for the making of a histamine aptamer-based biosensor. This is indicative that the histamine aptamer-based biosensor has the potential to be applied in various fields, which includes the detection of bed bugs, the medical diagnosis of allergy conditions, and the detection of maximum levels of toxic histamine in food and beverages in the food sector.

Table 4. 4 Chemical compounds and structural formulas of histidine, indole, tryptophan, pyrrole, and pyridine used as control colorimetric studies to determine binding specificity of aptamers towards target histamine.

Chemical Compounds	**Structural Formula**
Histamine (target)	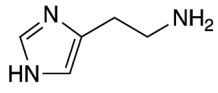
Histidine	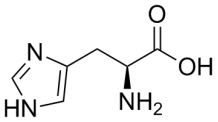
Indole	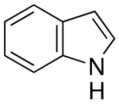
Tryptophan	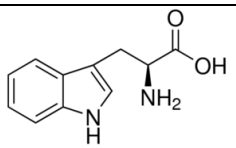
Pyrrole	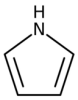
Pyridine	

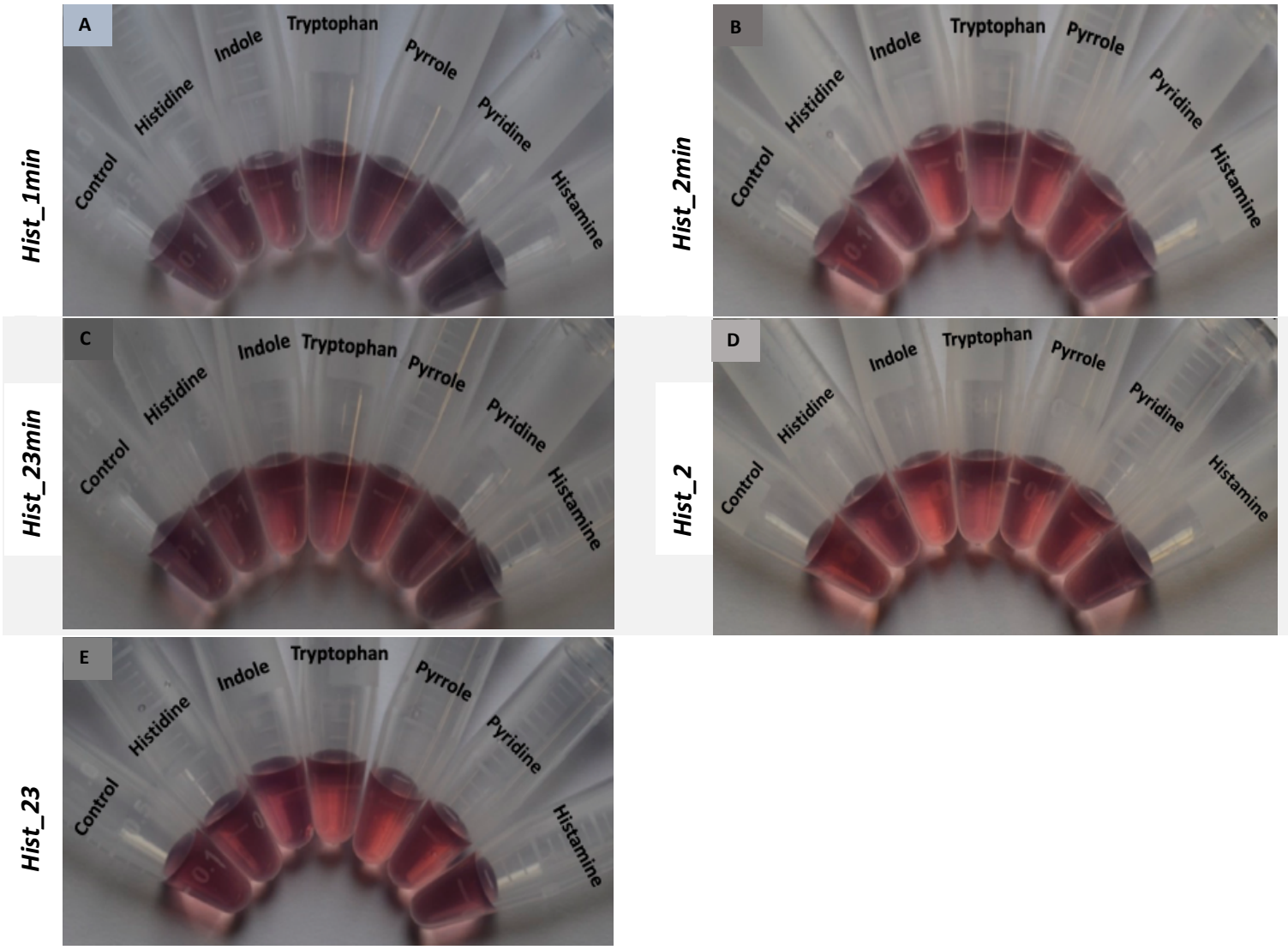

Figure 4.9 1 Photographs of the mixture of **(A)** Hist_1min AuNPs, **(B)** Hist_2min-AuNPs, **(C)**, Hist_23min-AuNPs, (**D)** Hist_2-AuNPs, **(E)** Hist_23-AuNPs solutions in the presence of 1.5 µM histidine, indole, tryptophan, pyrrole, pyridine and target histamine.

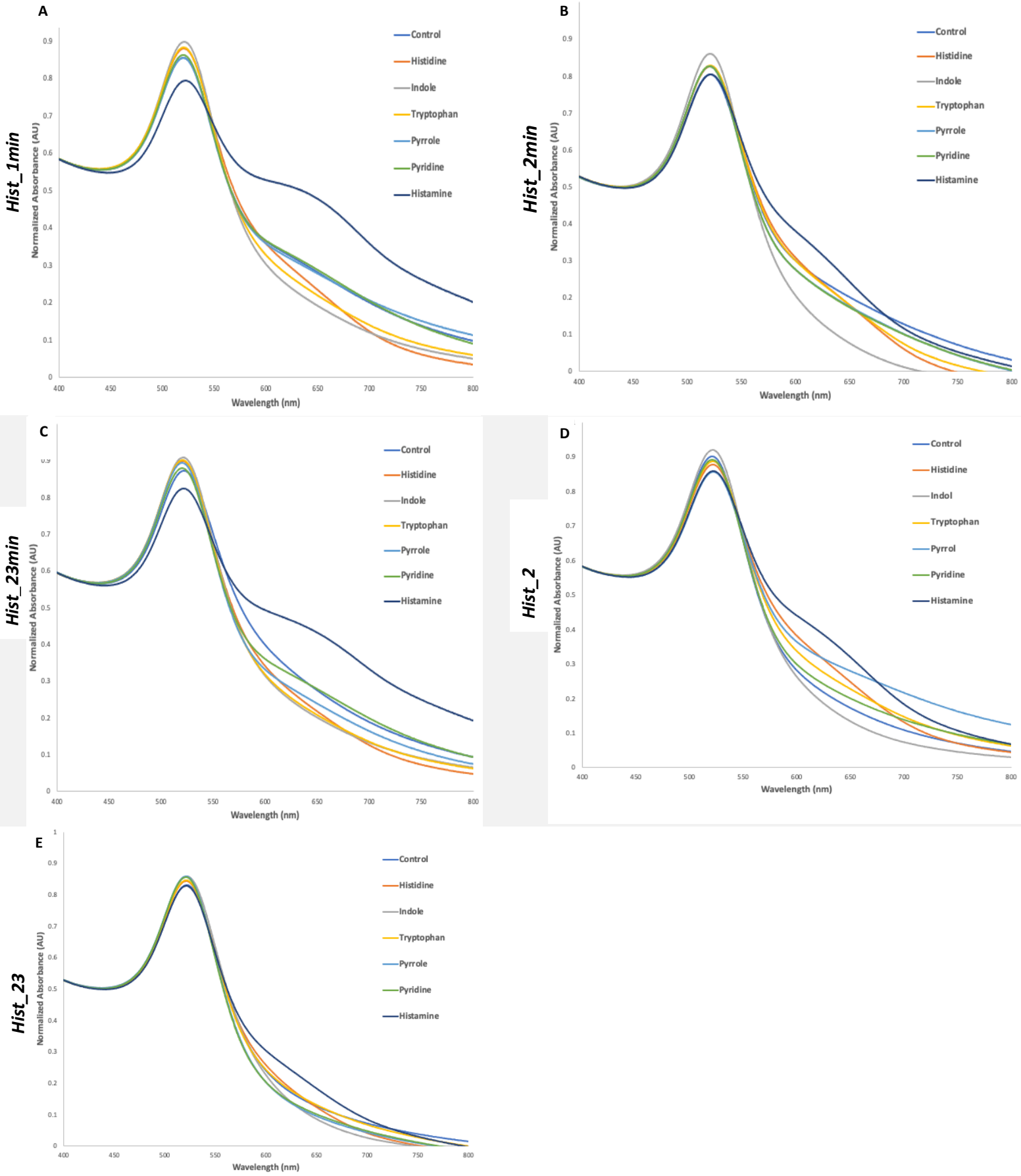

Figure 4.9 2 Spectral changes from the assembly of **(A)** Hist_1min-AuNPs, **(B)** Hist_2min-AuNPs, **(C)**, Hist_23min-AuNPs, (**D)** Hist_2-AuNPs, **(E)** Hist_23-AuNPs solutions in the presence of 1.5 µM histidine, indole, tryptophan, pyrrole, pyridine and target histamine.

4.10 Cy5 DNA Synthesis Quantification

The Beer-Lambert Law equation was used to determine the concentration of each aptamer using the measured absorbance value at λmax=256nm and the theoretical extinction coefficient. **Table 4.5** shows the calculated concentrations of each selected synthesized Cy5 labelled aptamers.

Table 4. 5 Cy5 labelled DNA quantification by UV/Vis at λmax=256 using a CARY 300 Bio spectrophotometer (Varian, USA)

Aptamer	Absorbance	Extinction Coefficient (L/mol·cm)	Concentration (mol/L) (10^{-6})	Concentration *DF (mol/L) (10^{-3})	nmol	Molecular Weight (g/mol)
Hist_23min	0.733	392300	1.868	3.737	78.5	12581.1
Hist_2	0.826	705500	1.171	2.342	58.5	22342.4
Hist_23	0.886	696400	1.272	2.545	101.8	22284.4

DNA synthesis was verified through molecular weight verification using electrospray ionization (ESI) mass spectrometry. As illustrated in **Figure 6.2 Appendix A**, the molecular ion peak obtained in all three aptamers confirmed the molecular weights as indicated in **Table 4.5**. Overall, these mass spectrum results demonstrated that the DNA synthesis was complete. However, the synthesized aptamers showed low purity as observed in the mass spectrum data. The Cy5 labeled aptamers were further purified by PAGE purification as shown in **Figure 6.4 Appendix B**.

4.11 MST Binding Studies of Histamine Aptamers

Further binding studies of the selected histamine aptamers were conducted through in-solution MST experiments. Selected fluorescently labelled Hist_2, Hist_23, and Hist_23min aptamers were run against target histamine ligand and control histidine ligand. The binding affinity of aptamers towards ligands were studied and the K_D values of aptamers were determined. As previously observed in the colorimetric assay results, the histamine aptamers showed some non-specific binding to histidine organic compound. In this MST binding experiment, further non-specific binding of aptamer towards histidine ligand was studied and evaluated.

In the binding affinity study of Hist_23 aptamer, binding was detected in the first of two technical runs in both histamine and histidine ligands. Common reasons for the second technical run to differ from the first run, is the degradation of the ligands (histamine and histidine). The ligands are degraded by the laser during the first run resulting to the lack of binding in the second run. Aptamers are stable enough to withstand degradation from the laser effect. A K_D value of 68 nM was reported towards target histamine ligand. A K_D value of 128 nM was also reported towards histidine ligand as shown in **Fig 4.11.1** and **Table 4.6**, confirming the presence of non-specific binding of the aptamer. As previously stated, this is potentially due to structural similarities between histamine target and histidine, with both compounds possessing an imidazole ring and an aliphatic amino group, with histidine differing by containing a carboxyl group as shown in **Table 4.4**. Histamine is mainly protonated at the aliphatic amino group at physiological conditions, contributing to the specific binding of histamine aptamers. In the case of histidine compound, the amino group is also protonated at physiological pH, which could contribute to the non-specific binding of histamine aptamer. However, the reported K_D value of Hist_23 aptamer towards target

histamine was 2x lower than histidine ligand, indicating that Hist_23 aptamer showed higher binding affinity towards target histamine ligand compared to histidine ligand. This is probably due to the differing histidine carboxyl group, which is deprotonated under physiological conditions.

Furthermore, Hist_23min aptamer binding was also detected in the first of two technical runs in both histamine and histidine ligands. A K_D value of 379 nM towards target histamine ligand was reported. These results indicate that the Hist_23 aptamer has a stronger binding affinity towards target histamine, compared to Hist_23min aptamer. The difference between the two aptamers is the absence of the primer regions in Hist_23min, which leads to a key finding of the importance of the primer regions involved in the binding towards its target. Aptamer Hist_23 that has the primer regions showed a stronger binding affinity towards target histamine compared to Hist_23min that lacks the primer regions.

In addition, Hist_23min also reported a K_D value of 400 nM towards histidine ligand confirming the presence of non-specific binding of this aptamer. The K_D value is also higher than the reported K_D value towards target histamine (379 nM), showing weaker binding towards histidine compared to histamine target. However, the difference is not significant to conclude that Hist_23min aptamer preferably binds to histamine compared to histidine.

Moreover, a negative correlation is observed in the binding isotherm of Hist_23min towards histidine ligand, as shown in **Figure 4.11.2 (b)**. Majority of cases, thermophoresis is positive, meaning that there is a net movement of molecules from hotter regions of the capillary to cooler regions. As a result, there is a net decrease in the observed fluorescence at the point of IR laser introduction. Negative thermophoresis may also occur, depending on the properties of the molecules [73]. The thermophoresis signal depends on the charge, size, and hydration shell of the aptamer. If the ligand binds to the aptamer, any of these

parameters change due to the presence of the ligand [65,73]. Different aptamers might respond with a different MST signal. Secondly, as a ligand binds to the aptamer, the temperature change of the fluorescence can be influenced by the ligand. Histidine ligand might induce a different MST signal when mixed with same Hist_23min aptamer, compared to histamine target ligand. The binding of the ligands (histamine and histidine) to the same aptamer, induces differing conformational change of the Hist_23min aptamer that results in contrasting thermophoresis signal.

Lastly, Hist_2 aptamer binding was detected in both two technical runs with target histamine. Interestingly, there was no apparent binding observed with histidine ligand as shown in **Figure 4.11.3 (b)**. An average K_D value of 1.29 μM was reported towards target histamine ligand. This thus shows that Hist_2 aptamer has a lower affinity towards target histamine ligand compared to both Hist_23 and Hist_23min aptamers. However, Hist_2 aptamer showed stronger binding specificity towards target histamine, as there was no apparent binding observed towards histidine ligand. Even though Hist_2 aptamer affinity is lower compared to other aptamers, the aptamer showed high specificity towards target histamine.

In conclusion, the MST experiments demonstrated which aptamers could potentially be selected for further biosensor assays. Aptamers Hist_2 and Hist_23 would be the most ideal for further binding studies, as these aptamers showed high affinity and specificity towards target histamine. These aptamers will further be applied to make an aptamer-based LFA biosensor that can readily be used to detect histamine levels in food and beverages, diagnose allergy related conditions, and detect bed bug infestation in various settings.

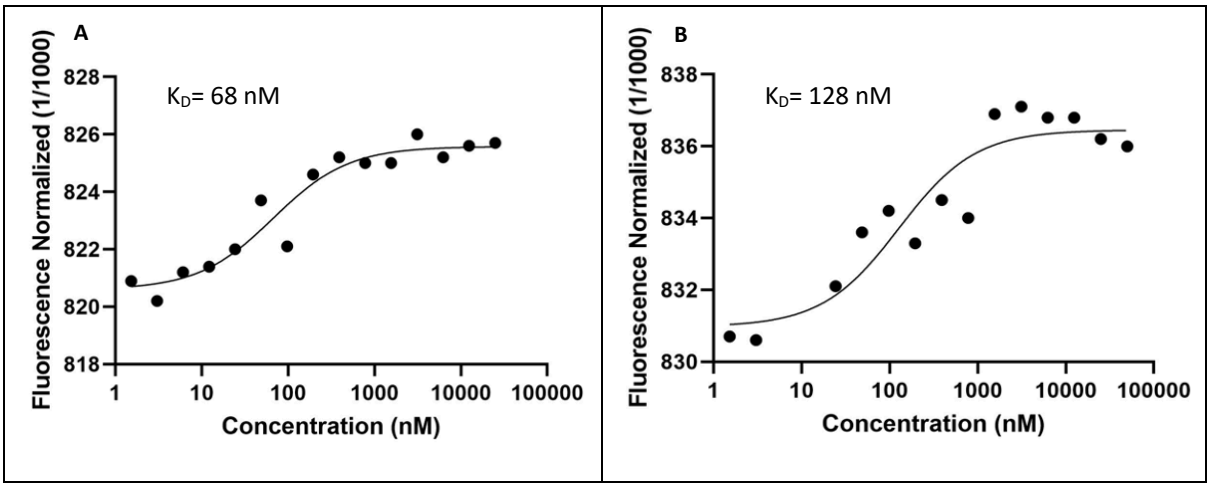

Figure 4.11. 1 Binding isotherms and reported K_D values for Hist_23 aptamer with ligand **(A)** Histamine, **(B)** Histidine obtained using MST.

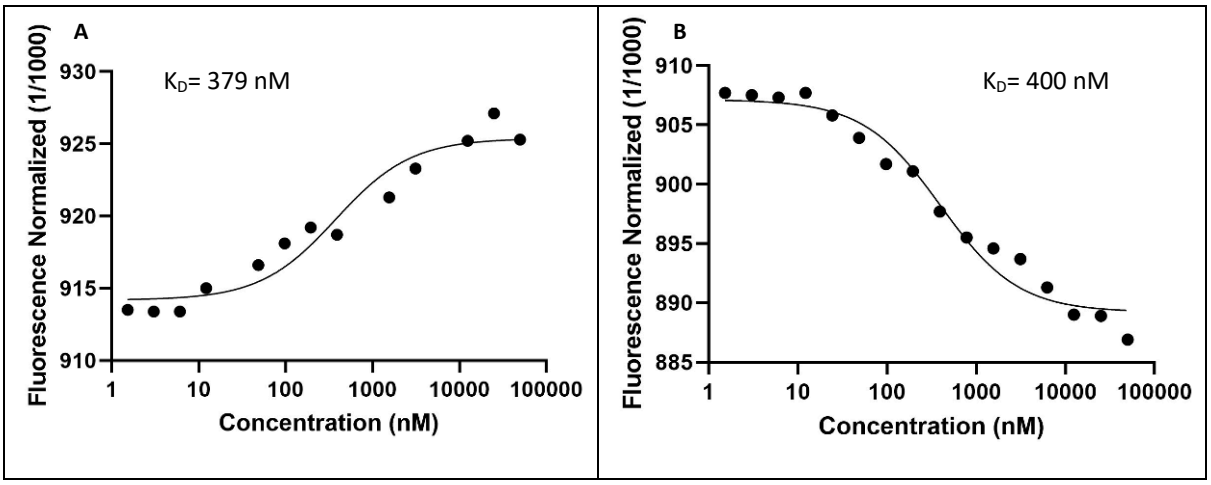

Figure 4.11. 2 Binding isotherms and reported K_D values for Hist_23min aptamer with ligand **(A)** Histamine, **(B)** Histidine obtained using MST.

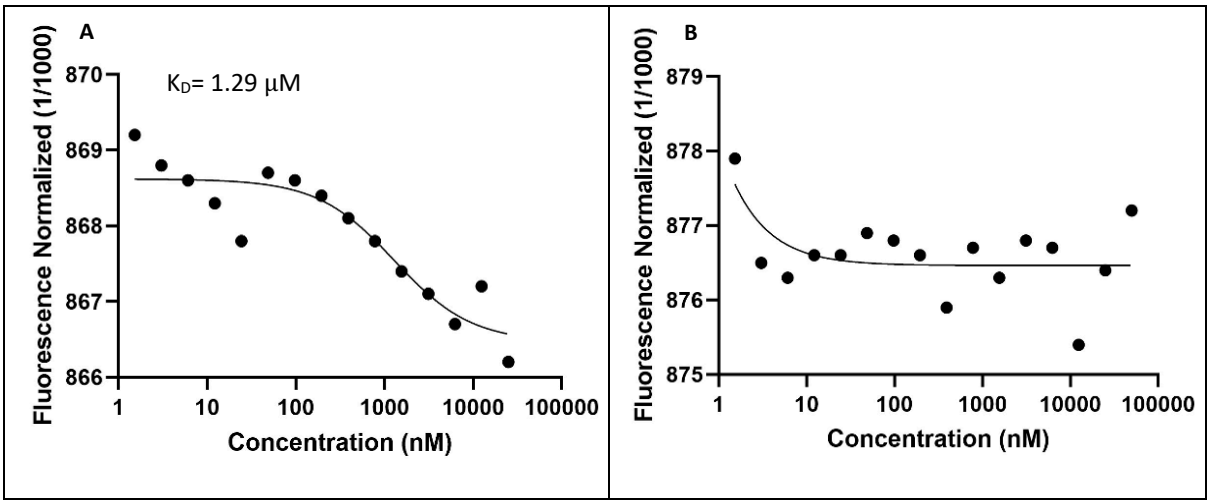

Figure 4.11. 3 Binding isotherms and reported K_D values for Hist_2 aptamer with ligand **(A)** Histamine, **(B)** Histidine obtained using MST.

Table 4. 6 Summary of reported K_D values for Hist_2, Hist_23, and Hist_23min aptamers with target histamine ligand, and control histidine ligand determined by MST.

Aptamer	**Target Histamine K_D**	**Control Histidine K_D**
Hist_23	68 nM	128 nM
Hist_23min	379 nM	400 nM
Hist_2	1.29 μM	No Binding

Chapter 5: Application of Histamine Aptamer-Based Biosensor

5.1 Introduction: Histamine Aptamer-Based Lateral Flow Assay

The detection of biogenic amine histamine has proven to be difficult due to its instability and low concentration in biological fluids. The structural similarities with other biogenic amines in biological fluids also hinders the accurate detection of histamine. As discussed previously, current methods of detection include, HPLC coupled with mass spectrometry, radioimmunoassays, and capillary electrophoresis coupled with mass spectrometry. These detection methods are expensive and require highly skilled workers which is not ideal for everyday testing. Moreover, commercial ELISA detection kits that are based on the use of antibodies, have frequently exhibited cross reactivity with other biogenic amines [36].

Currently, there are limited reported histamine-aptamer based biosensors that can readily be used as a point of care testing method. Among them are that described by Mairal Lerga et al, which reported a K_D value of 3∼34 nM, acquired by indirect binding assay. A histamine-magnetic beads competitive assay aptasensor was also assembled that achieved an LOD of 18 pM, and an LOD of 76 pM in the detection of histamine in synthetic urine [36]. Moreover, John Ho et al reported a histamine aptamer binding affinity of 72.8 nM

determined by a magnetic bead-based enzyme linked oligonucleotide assay. An EIS aptasensor further displayed an apparent binding affinity and LOD of 7.80 mM and 4.83 mM, respectively [50]. Furthermore, other studies such as Dwidar et al reported an RNA aptamer that specifically recognizes histamine with a K_D value of 370 nM acquired by ITC. An aptasensor based on the structure-switching mechanism was also developed that could detect histamine concentrations as low as 1 μM which was used to detect histamine levels in tuna samples [40].

Lateral flow assays (LFA) are a paper-based detection device that detects a wide range of targets in a matter of minutes. Due to their low development cost, and ability to detect targets rapidly with high specificity, they have been established for point-of-care applications in diverse fields including, food safety, environmental health, industry quality control, and medical diagnosis [48]. LFAs were first commercially launched in the 1980s as the urine-based pregnancy test [74]. This was followed by a flux of commercialized LFAs in diverse fields. In medical diagnosis, LFAs can be applied onto a range of biological samples including sweat, saliva, urine, and blood.

LFA is composed of different parts including sample pad, conjugate pad, nitrocellulose membrane, and a wicking or absorbent pad all assembled on a plastic pad. Conventionally, in the detection of target, a liquid sample is added onto the sample pad. The sample pad transports the sample to the conjugate pad via wicking. The conjugate pad contains labelled biorecognition molecules, which are released upon contact with the liquid sample as it moves through the nitrocellulose membrane by capillary action. The absorbent pad provides the capillary driving force, maintaining the flow rate of the liquid samples and preventing the back flow. Test and control lines are drawn over the nitrocellulose

membrane. Upon arrival on the test line, a visible color spot is formed when the liquid sample contains the target analyte [48].

The development of aptamer based LFAs functionalized with AuNPs has increased over the years, due to its ability to rapidly detect wide range of targets from small to large molecules with high specificity, and at a low cost. Such aptamer-based LFAs that have been developed, includes the detection of mycotoxins for food safety in the agriculture industry [45,46,51,75]. These developed aptasensors have proven to be highly sensitive and selective towards the target. They have also proved to be practical and applicable as a point-of care with no requirement of specialized personnel and equipment.

In this study, a “reverse adsorption-desorption” colorimetric LFA that detects histamine is developed. A lateral flow strip is prepared with streptavidin (binds to the biotin-labelled aptamer) at the test spot and a charged polymer at the control spot. Biotin-labelled histamine aptamers are initially incubated with or without target histamine, followed by the incubation of mixed solution with AuNPs as illustrated in **Figure 5.1.1**. In the absence of histamine target, biotin-labelled histamine aptamers are adsorbed onto the AuNP surfaces and captured by the streptavidin, which leads to the presence of a red spot on the test line. On the other hand, in the presence of target histamine, biotin labelled histamine aptamers are desorbed from AuNPs surfaces, as they preferably bind with target histamine that results to an absence of red spot observed on the test line. In this study a novel histamine aptamer-based later flow assay is developed, that will potentially revolutionize point of care testing in patients with allergy conditions. Moreover, this biosensor could potentially be used to detect maximum levels of histamine in food and alcoholic beverages. Further potential applications also include the detection of bed bug infestations in various settings.

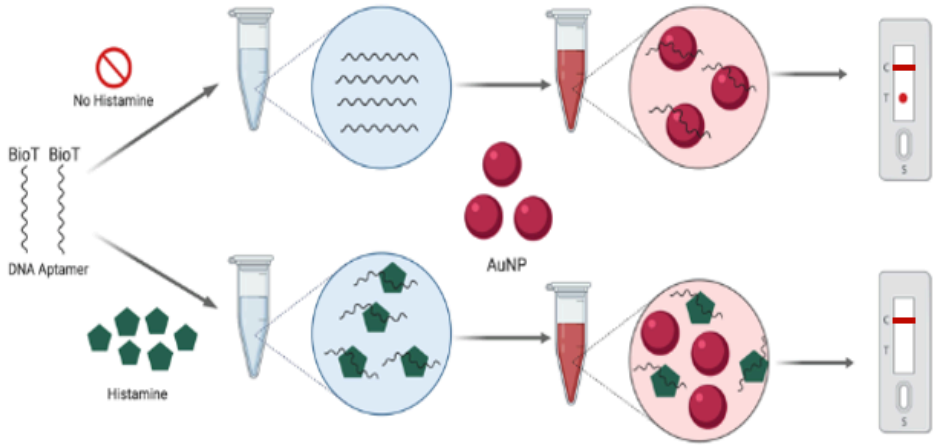

Figure 5.1. 1 Schematic illustration of LFA format. A lateral flow strip is prepared with streptavidin (binds to the biotin-labelled aptamer) at the test line and a charged polymer at the control line. Biotin-labelled histamine aptamers are incubated with or without target histamine, followed by the incubation of mixed solution with AuNPs. In absence of histamine target, biotin-labelled histamine aptamers are adsorbed onto the AuNPs surfaces and captured by the streptavidin, which leads to the presence of a red spot on the test line. In the presence of target histamine, biotin labelled histamine aptamers are desorbed from the AuNPs, as they preferably bind with target histamine. This results to an absence of red spot observed on the test line. *Figure was designed on BioRender*.

5.2 Materials and Methods

5.2.1 Materials and Instrumentation

Gold (III) chloride hydrate ($HAuCl_4.3H_2O$, ≤99.9%), sodium citrate, poly (diallyldi-methylammonium chloride) (PDDA, 200 000-350 000 Mwt, 10% solution), and streptavidin were purchased from Sigma-Aldrich. Histamine (2-(4-Imidazolyl) ethylamine, ≥97.0%) and L-Histidine monohydrochloride monohydrate were purchased from Sigma-Aldrich. Sample pad (CFSP223000, 20 cm x 30 cm), HiFlow Plus NC membrane (HFC18004, 30.5 cm x 25 cm), absorption pad (CFSP223000, 20 cm x 30cm) and conjugate pad (GFDX203000 20 cm x 30 cm) were purchased from Millipore Corporation, Bedford, MA. Ultrapure water was obtained from a Millipore Milli-Q deionized water system at 18 MΩ (Waters, Milford, MA,

USA). For quantitative analysis, the signal strength of test line to control line peak area ratio of the LFA was measured using the Image J software.

5.2.2 Biotin Modified Aptamer Synthesis

Biotin labelled 5' aptamer sequences Hist_2, and Hist_23 were prepared using standard phosphoramidite chemistry on a Bioautomation MerMade 6 DNA synthesizer (Plano, TX, USA). Oligonucleotides were labelled with 5'-Biotin Phosphoramidite (Glen Research). Aptamers were synthesized in a 3' to 5' direction through a repeating series of organic reactions. Hist_2 and Hist_23 sequences were all 71 based length aptamers containing identical 3' and 5' primers, and a randomized region indicated in **Table 5.1**.

The phosphoramidites, dA-CE, Ac-dC-CE, dmf-dG-CE, and dT-CE were obtained from Glen Research (Sterling, VA, USA). They were each dissolved in anhydrous acetonitrile (Glen Research) to create 0.1 μM solutions of each amidite in argon atmosphere. 5' Cyanine Dye was obtained from Glen Research (Sterling, VA, USA). Ultra-High Purity 5.0 argon was purchased from Praxair Canada (Mississauga, ON, Canada). The dissolved phosphoramidites were connected to the DNA synthesizer along with anhydrous acetonitrile (BDH VWR analytical), activator solution, deblock solution, cap A solution, cap B solution, and oxidizer solution all obtained from Glen Research (Sterling, VA, USA). The 1000 Å 1.0 μmole-controlled pore glass synthesis columns (Biautomaton) for each Hist_2 and Hist_23 aptamers contained an initial thymine. The columns were also connected to the DNA synthesizer. The appropriate script file was loaded on the MerMade software and synthesis was performed overnight.

Table 5. 1 Biotin labelled sequences of histamine aptamers with BioT modifier on 5' end.

Sequence Name	**Length (bases)**
Hist_2	71
Hist_23	71

5.2.3 Purification of 5'-Biotin labelled Synthetic Oligonucleotides

Following DNA synthesis, the 4,4'-dimethoxytrityl (DMT) oligonucleotides were ultrafast deprotected in a 1:1 mixture (v/v) of aqueous ammonium hydroxide and aqueous methylamine at 65℃ for 5 minutes. Once cooled at room temperature, a 1 mL of 100 mg/mL sodium chloride solution was added to the deprotected DMT-ON oligonucleotide for a final volume of 2 mL. The 150 mg Glen-Pak DNA Purification Cartridges (Glen Research) were conditioned using 0.5 mL of acetonitrile followed by 1 mL of 2 M TEAA on the vacuum pump. The acetonitrile washes organic residues from resin, while the TEAA acts as an ion-pairing reagent to enhance the binding of the DMT-ON oligonucleotide to the resin. The oligo/salt mixture was applied onto the cartridge in 1 mL aliquots. During the loading process, the DMT-ON oligos are bound to the cartridge, while failed sequences are not retained. The cartridge was then washed with 2 x 1 mL of salt wash solution (5% Acetonitrile in 100 mg/mL Sodium Chloride) to wash away the remainder of the failure sequences from the cartridge. This was followed by the rinsing of the cartridge with 2 x 1 mL of 2% TFA to

remove the DMT from the bound oligonucleotide. The oligo was left in contact with the TFA solution for 10 minutes due to 5'-Biotin being slow to detritylate. The cartridge was then washed with 2 x 1 mL of deionized water, rinsing away the TFA and excess salts. The purified oligos were eluted into sample tubes using 1 x 1 mL 50% acetonitrile in water with 0.5% ammonium hydroxide. The collected oligos were dried down by a SpeedVac overnight; an Automatic Environmental SpeedVac® System AES2010 (Savant).

5.2.4 Quantification of 5'-Biotin labelled Aptamers using UV-Vis Spectroscopy

Synthesized DNA concentration was determined using UV-Vis spectroscopy; a CARY 300 Bio spectrophotometer (Varian, USA). Aliquots of the DNA stock solutions were diluted with deionized water, in order to measure absorbances between 0.4-0.8 at 256 nm. The Beer-Lambert Law equation was used to determine the concentration of each aptamer using the measured absorbance value and the theoretical extinction coefficient, provided through the use of OligoAnalyzer® Tool, version 3.1, on the Integrated DNA Technologies (IDT) website (PrimerQuest® program, IDT, Coralville, Iowa, USA). The aptamers were diluted and stored at -20℃.

The purity of the aptamer was determined through molecular weight verification by mass spectrometry. Samples of 1 nmol of the aptamer solution were dried using the SpeedVac and sent to Novatia for ESI mass spectrometry analysis.

5.2.5 Preparation of AuNPs and Test Solutions for Reverse Adsorption-Desorption Method

Samples were prepared by adding 8 μL of 5'-biotin-modified aptamer (10 μM stock in water) to histamine target prepared in water at final concentrations ranging from 1 nM to 500 nM and incubated for 30 minutes. AuNP (50 μL aliquot of 11.77 nM) solution was added

into each microcentrifuge tube containing aptamer-target solution and vortexed briefly, followed by a 30 minutes incubation period.

5.2.6 Preparation of the Lateral Flow Assay

The LFA is composed of four overlapping pads: sample pad, conjugate pad, membrane and absorption pad. All pads were cut into strips of 5 mm using a paper cutter, which were placed on a plastic adhesive backing. The four pads were assembled from top to bottom as follows: absorption pad, HiFlow Plus membrane, glass fiber conjugation pad, and sample pad. Each pad overlaps 2 mm to allow the migration of sample solution along the LFA during the analysis. Streptavidin, used as a capture reagent, was applied (2.5 mg/mL, 0.5 μL) on the membrane as a thin dot (test spot) and the whole device was then dried 30 minutes at room temperature before use.

In the "reverse adsorption-desorption" colorimetric lateral flow assay, a control line (10% PDDA polymer, 0.5 μL) was applied on the nitrocellulose membrane, which can non-specifically trap AuNPs. Streptavidin, used as a capture reagent, was applied (2.5 mg/mL, 0.5 μL) on the membrane as a test dot. The sample solutions contained the mixture of aptamer-AuNPs conjugate, with the presence of increasing concentrations of histamine target. The test solutions were applied to the sample pad (40 μL) and the device was read after a minute. The absence of the colored test spot was indicative of histamine presence. Color at the control line confirmed that nanoparticles did migrate effectively across the device.

5.3 Results and Discussion

5.3.1 5' Biotin-modified DNA Synthesis Quantification

The Beer-Lambert Law equation was used to determine the concentration of each aptamer using the measured absorbance value at λmax=256 and the theoretical extinction coefficient. **Table 5.2** shows the calculated concentrations of each synthesized Biotin-modified aptamer.

Table 5. 2 Biotin-modified DNA quantification by UV/Vis at λmax=256 using a CARY 300 Bio spectrophotometer (Varian, USA)

Aptamer	Absorbance	Extinction Coefficient (L/mol·cm)	Concentration (mol/L) (10^{-7})	Concentration *DF (mol/L) (10^{-3})	nmol	Molecular Weight (g/mol)
Hist_2	0.334	705500	4.734	0.473	189.4	22747.85
Hist_23	0.405	696400	5.816	0.582	232.6	22689.85

DNA synthesis was verified through molecular weight verification using electrospray ionization (ESI) mass spectrometry. As illustrated in **Figure 6.3 Appendix A**, the molecular ion peak obtained in all two biotin-labelled aptamers confirmed the molecular weights as indicated in **Table 5.2**. Overall, these mass spectrum results demonstrated that the DNA synthesis was complete.

5.3.2 Histamine Aptamer-based Colorimetric Lateral Flow Assay

A histamine aptamer-based colorimetric adsorption-desorption lateral flow assay was performed in this study. It is important to note that only Hist_23 aptamer was studied in this

experiment over two trials due to time constraint. Initially, a series of optimizations of AuNP, aptamer and streptavidin concentrations were performed. Building upon the reverse colorimetric adsorption-desorption assay, a similar mechanism occurred in this assay. Biotin-modified Hist_23 aptamer was initially incubated with increasing concentration of target histamine, followed by the incubation of mixture with AuNPs solution. In the presence of histamine, biotin-modified Hist_23 aptamers are desorbed from the AuNP surface, as they preferably bind specifically onto target.

In the absence of histamine target, the biotin-modified Hist_23-AuNP complex can migrate along the membrane and be captured by streptavidin to form a red spot on the test line. Furthermore, a red color line is also observed at the polycation (PDDA) control line, as the positively charged PDDA will non-specifically trap the negatively charged AuNPs via electrostatic interaction. This confirms that the solution has successfully migrated along the membrane.

In the presence of increasing concentration of histamine target (0-500 nM), the biotin-modified Hist_23 aptamers are desorbed from the AuNP surface, as they are specifically bound to target histamine. As the mixture solution migrates along the membrane, the biotin-modified Hist_23-histamine target complex is captured by the streptavidin. As the complex lack the AuNPs, a gradual decrease in red color intensity was observed on the test line as the concentration of histamine increased as shown in **Figure 5.3.2.1**. A red line was also observed at the control line, due to the presence of PDDA capturing the AuNPs which confirmed the successful migration of the solution along the membrane. The peak areas on the test line and control line were analyzed using ImageJ software and a calibration curve was plotted as the percentage peak area intensity of test and control line (T/C+T) vs increasing concentration of histamine target as shown in **Figure 5.3.2.2**. As observed in the

figures below, the red spot intensity on the test line drastically decreased when the concentration of histamine increased to 10 nM. Thereafter, the intensity on the test line plateaued as the concentration of histamine increased, and no complete disappearance of red spot was observed on the test line. At the same time there was a significant increase in intensity on the control line as the concentration of histamine increased to 10 nM. This observed trend occurred as a result of the PDDA on the control line capturing the amount of AuNPs that were initially captured on the test line when no target histamine was present, hence supporting the mechanism of the assay. Since the intensity on the test line drastically decreased as the concentration of histamine increased to 10 nM, and generally plateaued thereafter, one can therefore determine the apparent LOD to be below 10 nM. The developed aptasensor could potentially be more sensitive in comparison with other reported histamine aptasensors, with the apparent LOD being lower than that of Dwidar et al and John Ho et al, which reported an LOD of 1 μM and 4.83 mM, respectively [40,50]. However, the apparent LOD was higher compared to that described by Mairal Lerga et al, which reported an LOD of 18 pM [36]. Nevertheless, the developed histamine LFA aptasensor is more rapid and easier to use in comparison to other histamine aptasensors.

Overall, these results are promising but further optimizations are recommended. Such optimizations include lowering the concentration of streptavidin. The current concentration of streptavidin might potentially cause some non-specific interaction with the AuNP surface, hence resulting in the persistence of a red spot on the test line. One could also modify the surface of AuNPs, to minimize non-specific interaction with streptavidin. Other optimization avenues include the alteration of AuNP and aptamer concentrations. For future studies, it is recommended to study at histamine concentrations below 10 nM to determine the LOD of

the LFA strip. These improvements of the assay can potentially make the strip more sensitive and achieve a lower limit of detection.

In general, the histamine aptamer-based LFA has demonstrated its ability to detect histamine target rapidly within an 1 hour with high sensitivity. This “signal off” approach can be read with the naked eye in less than 5 minutes. One limitation of this potential histamine-aptamer based biosensor, is the necessity of a specialized reader, to measure and analyze the results. However, due to the cost-effectiveness of the strip, the biosensor is commercially viable and can potentially be applied as a point-of-care detection tool in diverse fields including, food safety, medical diagnosis of allergy related conditions, and for the detection of bed bugs.

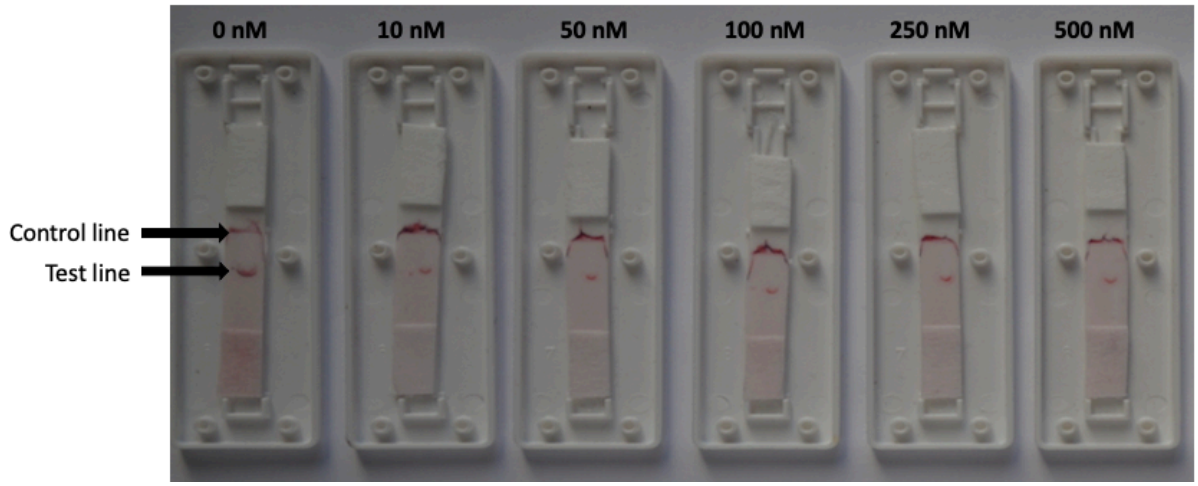

Figure 5.3.2. 1 Histamine aptamer-based adsorption-desorption lateral flow assay for the detection of increasing histamine concentration (0-500 nM). In the absence of histamine target, biotin-labelled Hist_23 aptamers are adsorbed onto the AuNP surfaces, that leads to the capture of Hist_23 aptamer-AuNPs conjugate onto the streptavidin membrane. This resulted in a red color dot observed on the test line. In the presence of target histamine, biotin labelled Hist_23 aptamers are desorbed from AuNPs as they preferably bind with target histamine. As a result, a gradual decrease in red color intensity is observed on the test line.

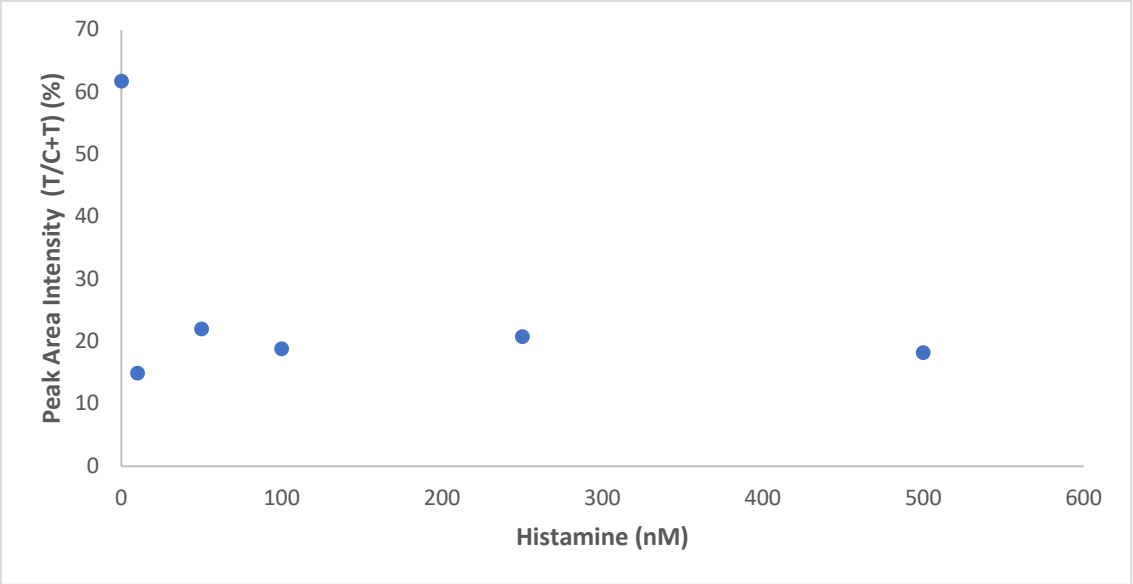

Figure 5.3.2. 2 Calibration curve of the percentage peak area intensity of test and control line (T/C+T) vs increasing concentration of histamine target, for the Hist_23 aptamer-based adsorption-desorption lateral flow assay.

Conclusion

Histamine aptamers were characterized in solution with target histamine by colorimetric binding assay and microscale thermophoresis. A head-to-head comparison of binding affinity and specificity for these group of aptamers were conducted, and the aptamer candidate better suited for biosensor application was selected. The aptamer-based colorimetric assay proved it was a rapid, highly sensitive, and relatively inexpensive detection method, with results visible with the naked eye. Aptamers Hist_2, Hist_23, and Hist_23min were selected out of the five aptamers due to their high affinity and specificity towards histamine target. Further binding studies of these selected aptamers were conducted through microscale thermophoresis. The rapid measurements and low sample consumption use makes MST an ideal aptamer characterization method. Aptamers Hist_2 and Hist_23 were selected due to the observed specificity and strong affinity towards target histamine giving a K_D of 1.29 µM and 68 nM, respectively. These selected aptamers were

best suited for an aptamer-based lateral flow assay biosensor. Although further LFA optimizations are recommended, the developed LFA aptasensor proved to be highly sensitive, with results visible with the naked eye. Its versatility and low cost make it a practical aptasensor that can be applied as a point-of care testing tool in various settings.

Appendices

Appendix A: Mass Spectra of Histamine Aptamers

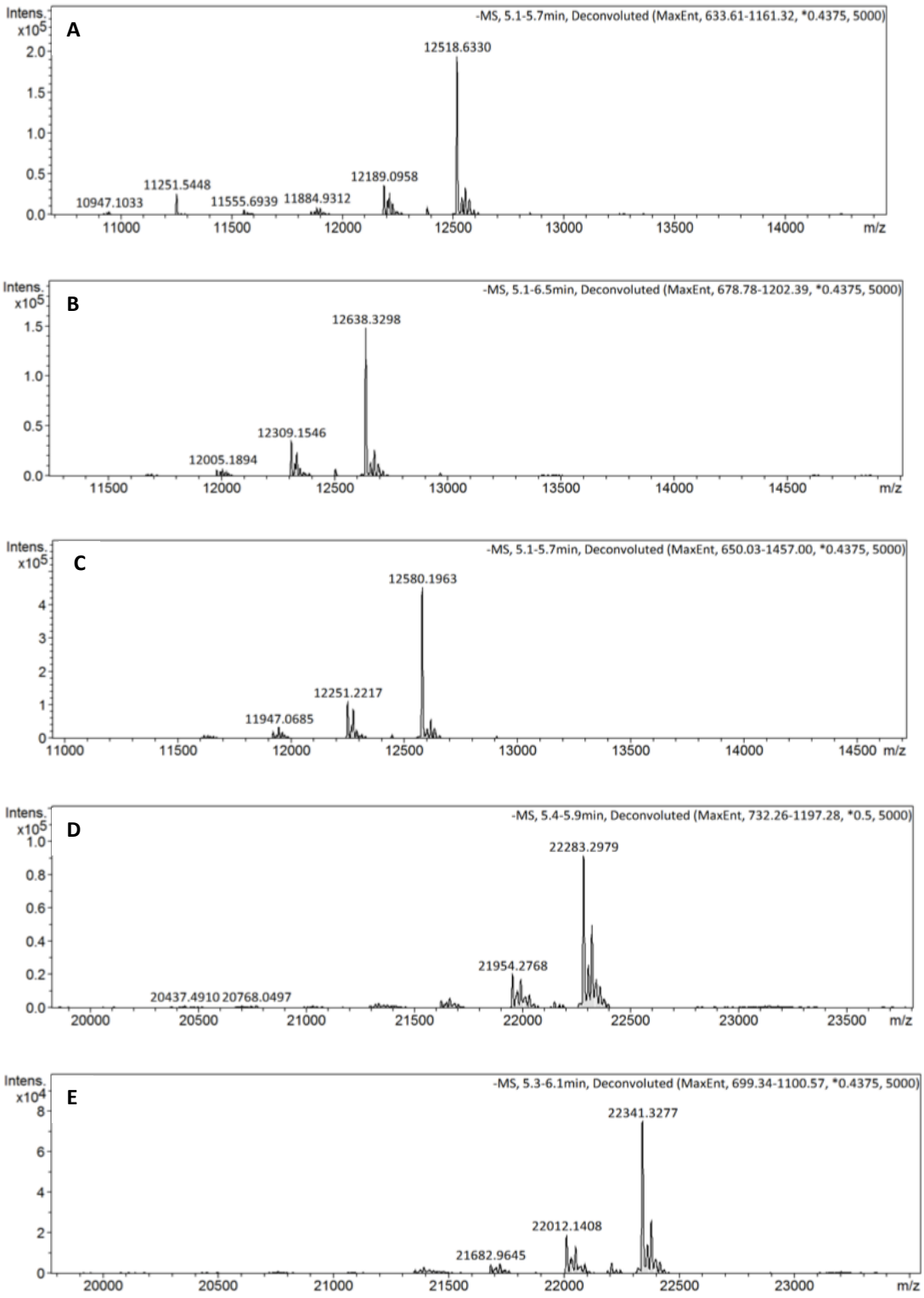

Figure 6. 1 Mass spectrum analysis of **(A)** Hist_1min, **(B)** Hist_2min, **(C)** Hist_23min, **(D)** Hist_2, **(E)** Hist_23 aptamers using McGill ESI mass spectrometry.

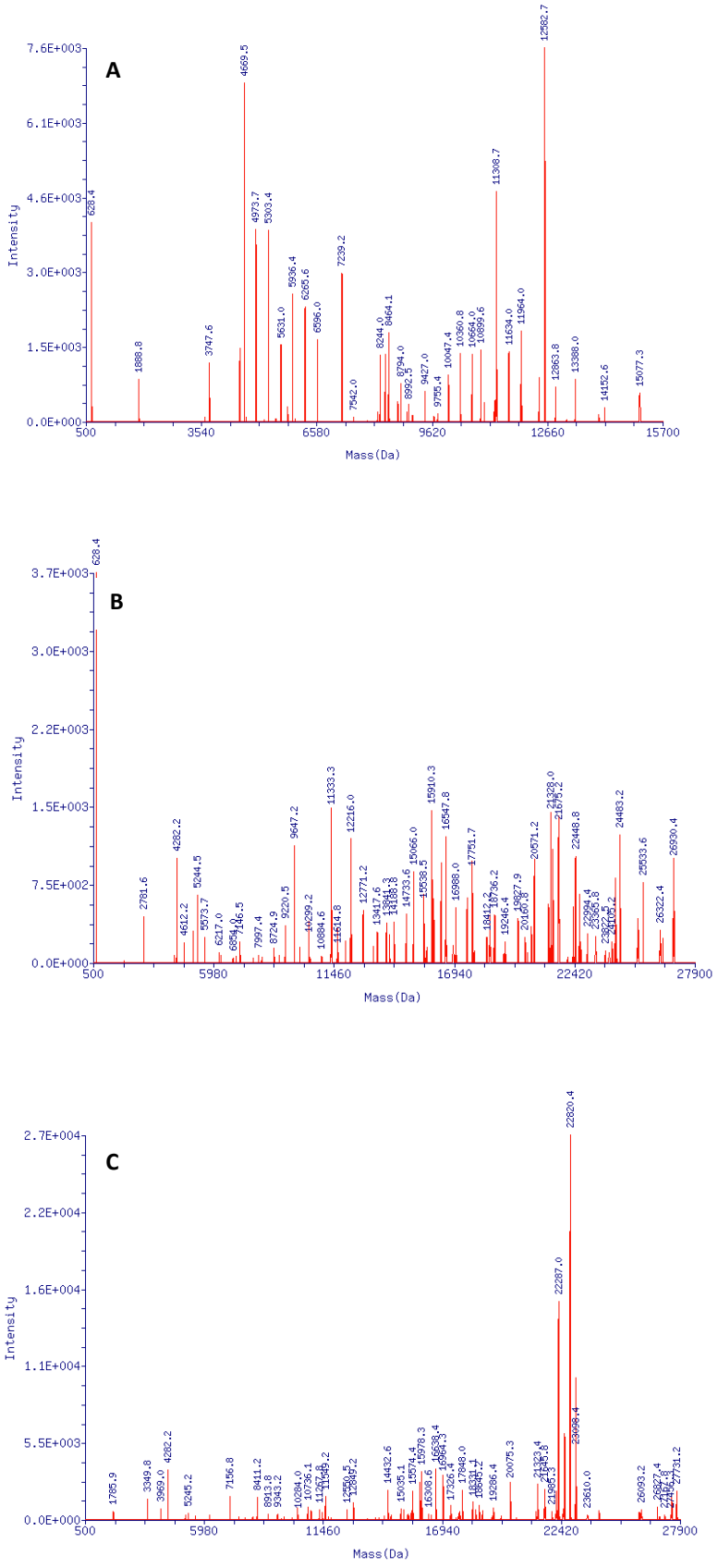

Figure 6. 2 Mass spectrum analysis of 5' cyanine dye labelled **(A)** Hist_23min, **(B)** Hist_2, **(C)** Hist_23 aptamers using Novatia electrospray ionization (ESI) mass spectrometry.

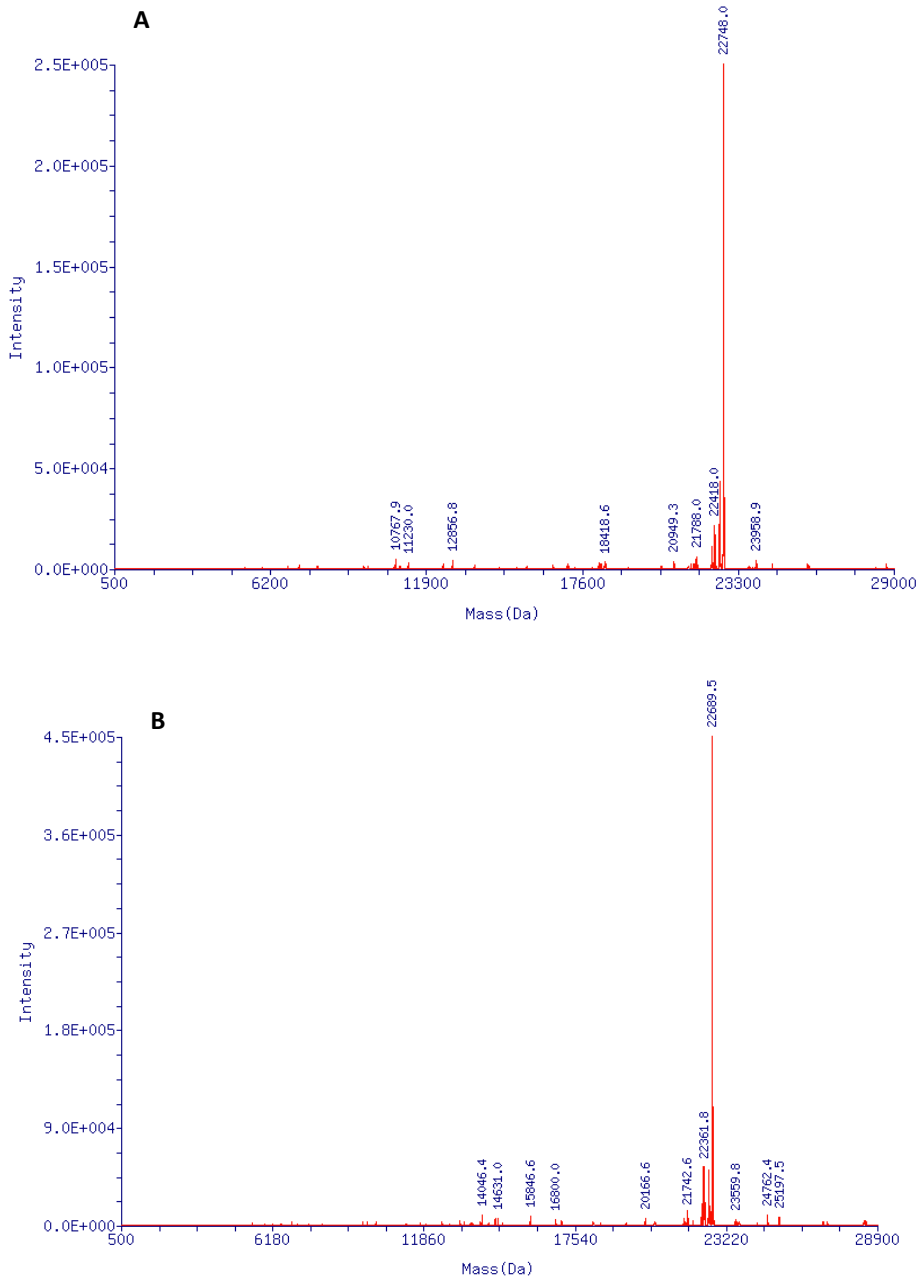

Figure 6. 3 Mass spectrum analysis of 5' BioT modified **(A)** Hist_2, **(B)** Hist_23 aptamers using Novatia electrospray ionization (ESI) mass spectrometry.

Appendix B: PAGE Purification Gel Images of 5’ Cyanine Dye Synthetic Oligonucleotides

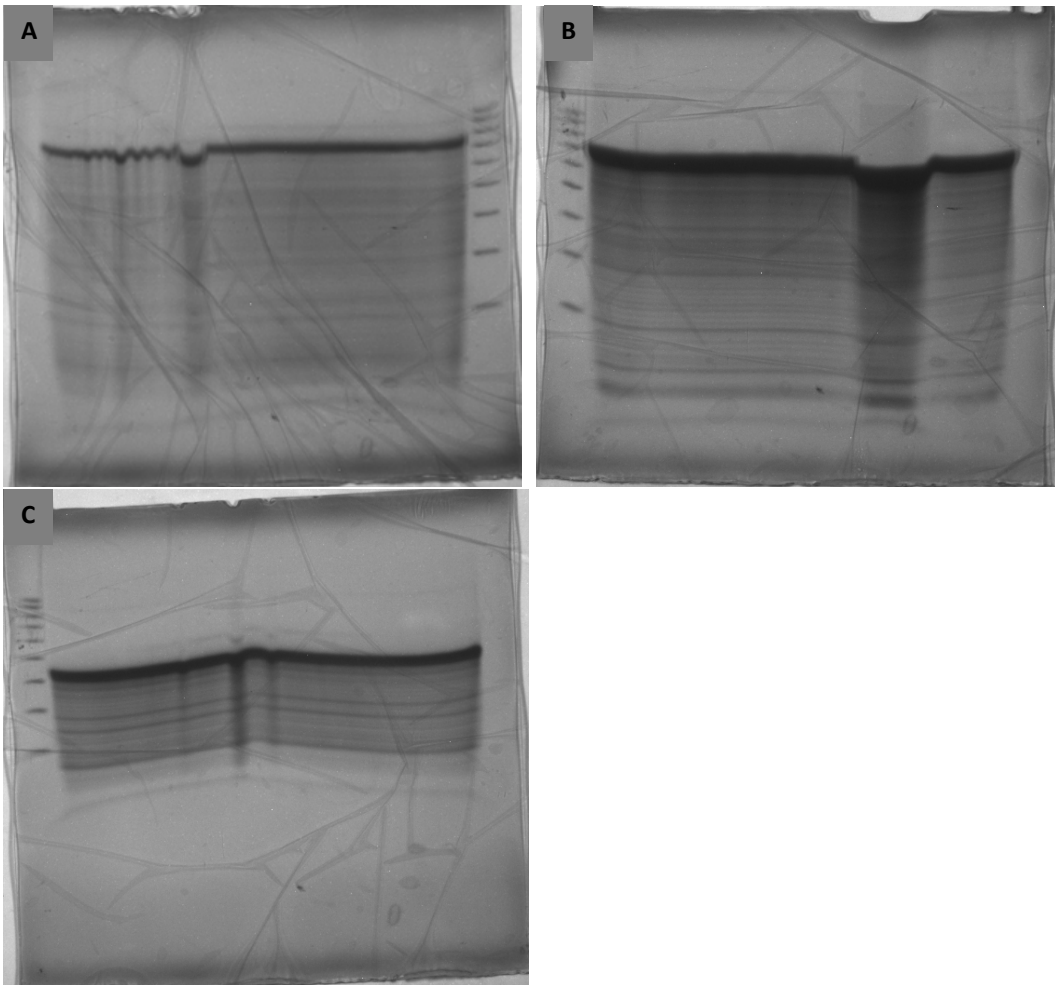

Figure 6. 4 PAGE purification gel images of 5’ cyanine dye labelled **(A)** Hist_2, **(B)** Hist_23, **(C)** Hist_23 min aptamers using Alpha Imager (AlphaEaseFC).

References

[1] K. Kabashima *et al.*, 'Biomarkers for evaluation of mast cell and basophil activation', *Immunol. Rev.*, vol. 282, no. 1, pp. 114–120, Mar. 2018, doi: 10.1111/imr.12639.

[2] T. B. Paiva, Mineko. Tominaga, and A. C. M. Paiva, 'Ionization of histamine, N-acetylhistamine, and their iodinated derivatives', *J. Med. Chem.*, vol. 13, no. 4, pp. 689–692, Jul. 1970, doi: 10.1021/jm00298a025.

[3] M. Gagic, E. Jamroz, S. Krizkova, V. Milosavljevic, P. Kopel, and V. Adam, 'Current Trends in Detection of Histamine in Food and Beverages', *J. Agric. Food Chem.*, vol. 67, no. 3, pp. 773–783, Jan. 2019, doi: 10.1021/acs.jafc.8b05515.

[4] 'Histidine decarboxylase', *Wikipedia*. Nov. 19, 2020, Accessed: Nov. 22, 2020. [Online]. Available: https://en.wikipedia.org/w/index.php?title=Histidine_decarboxylase&oldid=989554035.

[5] Z. C. DeVries, R. G. Santangelo, A. M. Barbarin, and C. Schal, 'Histamine as an emergent indoor contaminant: Accumulation and persistence in bed bug infested homes', *PLOS ONE*, vol. 13, no. 2, p. e0192462, Feb. 2018, doi: 10.1371/journal.pone.0192462.

[6] N. Gordon, L. O'Shaughnessy, D. Fitzpatrick, S. Doyle, and B. Mitchell, 'A Two Pronged Approach to the Detection of Cimex Lectularius (common bed bug) Using Novel Bed Bug Proteins', *J. Allergy Clin. Immunol.*, vol. 137, no. 2, p. AB32, Feb. 2016, doi: 10.1016/j.jaci.2015.12.105.

[7] R. Gries, R. Britton, M. Holmes, H. Zhai, J. Draper, and G. Gries, 'Bed Bug Aggregation Pheromone Finally Identified', *Angew. Chem.*, vol. 127, no. 4, pp. 1151–1154, Jan. 2015, doi: 10.1002/ange.201409890.

[8] R. Gries, H. Zhai, A. R. Lewis, R. Britton, and G. Gries, 'Common bed bugs can biosynthesize pheromone components from amino acid precursors in human blood', *Can. J. Chem.*, vol. 96, no. 2, pp. 212–216, Feb. 2018, doi: 10.1139/cjc-2017-0407.

[9] A. Ko and D.-H. Choe, 'Development of a lateral flow test for bed bug detection', *Sci. Rep.*, vol. 10, no. 1, p. 13376, Dec. 2020, doi: 10.1038/s41598-020-70200-0.

[10] R. Vaidyanathan and M. F. Feldlaufer, 'Bed Bug Detection: Current Technologies and Future Directions', *Am. J. Trop. Med. Hyg.*, vol. 88, no. 4, pp. 619–625, Apr. 2013, doi: 10.4269/ajtmh.12-0493.

[11] 'Can Bed Bug Traps Clear An Infestation?', *Popular Science*. https://www.popsci.com/can-bed-bug-traps-clear-infestation/ (accessed Nov. 23, 2020).

[12] U. R. Müller and G. Haeberli, 'The problem of anaphylaxis and mastocytosis', *Curr. Allergy Asthma Rep.*, vol. 9, no. 1, pp. 64–70, Jan. 2009, doi: 10.1007/s11882-009-0010-9.

[13] S. G. O. Johansson *et al.*, 'Revised nomenclature for allergy for global use: Report of the Nomenclature Review Committee of the World Allergy Organization, October 2003', *J. Allergy Clin. Immunol.*, vol. 113, no. 5, pp. 832–836, May 2004, doi: 10.1016/j.jaci.2003.12.591.

[14] H. A. Sampson *et al.*, 'Second symposium on the definition and management of anaphylaxis: Summary report—Second National Institute of Allergy and Infectious Disease/Food Allergy and Anaphylaxis Network symposium', *J. Allergy Clin. Immunol.*, vol. 117, no. 2, pp. 391–397, Feb. 2006, doi: 10.1016/j.jaci.2005.12.1303.

[15] T. Gülen, H. Hägglund, B. Dahlén, and G. Nilsson, 'High prevalence of anaphylaxis in patients with systemic mastocytosis - a single-centre experience', *Clin. Exp. Allergy*, vol. 44, no. 1, pp. 121–129, Jan. 2014, doi: 10.1111/cea.12225.
[16] T. Gülen, C. Ljung, G. Nilsson, and C. Akin, 'Risk Factor Analysis of Anaphylactic Reactions in Patients With Systemic Mastocytosis', *J. Allergy Clin. Immunol. Pract.*, vol. 5, no. 5, pp. 1248–1255, Sep. 2017, doi: 10.1016/j.jaip.2017.02.008.
[17] A. Górska *et al.*, 'Risk factors for anaphylaxis in patients with mastocytosis', *Pol. Arch. Intern. Med.*, vol. 125, no. 1–2, pp. 46–53, Jan. 2015, doi: 10.20452/pamw.2644.
[18] C. Akin, P. Valent, and D. D. Metcalfe, 'Mast cell activation syndrome: Proposed diagnostic criteria', *J. Allergy Clin. Immunol.*, vol. 126, no. 6, pp. 1099-1104.e4, Dec. 2010, doi: 10.1016/j.jaci.2010.08.035.
[19] T. C. Theoharides, P. Valent, and C. Akin, 'Mast Cells, Mastocytosis, and Related Disorders', *N. Engl. J. Med.*, vol. 373, no. 2, pp. 163–172, Jul. 2015, doi: 10.1056/NEJMra1409760.
[20] P. Valent *et al.*, 'Advances in the Classification and Treatment of Mastocytosis: Current Status and Outlook toward the Future', *Cancer Res.*, vol. 77, no. 6, pp. 1261–1270, Mar. 2017, doi: 10.1158/0008-5472.CAN-16-2234.
[21] P. Valent *et al.*, 'Diagnostic criteria and classification of mastocytosis: a consensus proposal', *Leuk. Res.*, vol. 25, no. 7, pp. 603–625, Jul. 2001, doi: 10.1016/S0145-2126(01)00038-8.
[22] P. Valent, C. Akin, and M. Arock, 'Diagnosis and Treatment of Anaphylaxis in Patients with Mastocytosis', *Curr. Treat. Options Allergy*, vol. 1, no. 3, pp. 247–261, Sep. 2014, doi: 10.1007/s40521-014-0021-1.
[23] P. Valent, C. Akin, and D. D. Metcalfe, 'Mastocytosis: 2016 updated WHO classification and novel emerging treatment concepts', *Blood*, vol. 129, no. 11, pp. 1420–1427, Mar. 2017, doi: 10.1182/blood-2016-09-731893.
[24] M. Castells, 'Diagnosis and management of anaphylaxis in precision medicine', *J. Allergy Clin. Immunol.*, vol. 140, no. 2, pp. 321–333, Aug. 2017, doi: 10.1016/j.jaci.2017.06.012.
[25] A. P. Almeida, W. Flye, D. Deveraux, Z. Horakova, and M. A. Beaven, 'Distribution of histamine and histaminase (Diamine oxidase) in blood of various species', *Comp. Biochem. Physiol. Part C Comp. Pharmacol.*, vol. 67, no. 2, pp. 187–190, Jan. 1980, doi: 10.1016/0306-4492(80)90014-3.
[26] E. B. Thangam *et al.*, 'The Role of Histamine and Histamine Receptors in Mast Cell-Mediated Allergy and Inflammation: The Hunt for New Therapeutic Targets', *Front. Immunol.*, vol. 9, p. 1873, Aug. 2018, doi: 10.3389/fimmu.2018.01873.
[27] E. B. Thangam *et al.*, 'The Role of Histamine and Histamine Receptors in Mast Cell-Mediated Allergy and Inflammation: The Hunt for New Therapeutic Targets', *Front. Immunol.*, vol. 9, p. 1873, Aug. 2018, doi: 10.3389/fimmu.2018.01873.
[28] B. S. Friedman, S. C. Steinberg, W. J. Meggs, M. A. Kaliner, M. Frieri, and D. D. Metcalfe, 'Analysis of plasma histamine levels in patients with mast cell disorders', *Am. J. Med.*, vol. 87, no. 6, pp. 649–654, Dec. 1989, doi: 10.1016/S0002-9343(89)80398-5.
[29] M. Raithel *et al.*, 'Excretion of urinary histamine and N-tele methylhistamine in patients with gastrointestinal food allergy compared to non-allergic controls during an unrestricted diet and a hypoallergenic diet', *BMC Gastroenterol.*, vol. 15, no. 1, p. 41, Dec. 2015, doi: 10.1186/s12876-015-0268-4.

[30] B. Patel and R. Divekar, 'Urinary N-methyl histamine levels relate to the presence of angioedema and decrease with the duration of chronic urticaria', *J. Allergy Clin. Immunol. Pract.*, vol. 5, no. 1, pp. 201–203, Jan. 2017, doi: 10.1016/j.jaip.2016.09.036.
[31] G. Myers, M. Donlon, and M. Kaliner, 'Measurement of urinary histamine: Development of methodology and normal values', *J. Allergy Clin. Immunol.*, vol. 67, no. 4, pp. 305–311, Apr. 1981, doi: 10.1016/0091-6749(81)90026-9.
[32] C. Bruce, R. Weatherstone, A. Seaton, and W. H. Taylor, 'Histamine levels in plasma, blood, and urine in severe asthma, and the effect of corticosteroid treatment.', *Thorax*, vol. 31, no. 6, pp. 724–729, Dec. 1976, doi: 10.1136/thx.31.6.724.
[33] D. Laroche and J.-M. Malinovsky, 'Diagnostic Value of Histamine and Tryptase Concentrations in Severe Anaphylaxis with Shock or Cardiac Arrest during Anesthesia', *Perioper. Med.*, p. 8.
[34] 'Histamine ELISA kit I Plasma & Urine Samples I 280€'. https://www.immusmol.com/histamine-elisa-kit-plasma-urine-detection.html (accessed Nov. 23, 2020).
[35] 'Histamine release kit I Whole Blood ELISA add-on kit'. https://www.immusmol.com/histamine-release-elisa-kit-whole-blood.html (accessed Nov. 23, 2020).
[36] T. Mairal Lerga *et al.*, 'High Affinity Aptamer for the Detection of the Biogenic Amine Histamine', *Anal. Chem.*, vol. 91, no. 11, pp. 7104–7111, Jun. 2019, doi: 10.1021/acs.analchem.9b00075.
[37] 'Hives Symptoms, Treatment, Causes, Home Remedies & Pictures'. https://www.medicinenet.com/hives/article.htm (accessed Nov. 23, 2020).
[38] 'What is Gastric Acid (Stomach Acid)? Is It Diluted When We Drink Water?' https://www.scienceabc.com/humans/is-your-stomach-acid-gastric-acid-diluted-when-you-drink-water.html (accessed Nov. 23, 2020).
[39] M. Papageorgiou, D. Lambropoulou, C. Morrison, E. Kłodzińska, J. Namieśnik, and J. Płotka-Wasylka, 'Literature update of analytical methods for biogenic amines determination in food and beverages', *TrAC Trends Anal. Chem.*, vol. 98, pp. 128–142, Jan. 2018, doi: 10.1016/j.trac.2017.11.001.
[40] M. Dwidar and Y. Yokobayashi, 'Development of a histamine aptasensor for food safety monitoring', *Sci. Rep.*, vol. 9, no. 1, p. 16659, Dec. 2019, doi: 10.1038/s41598-019-52876-1.
[41] G. Liu, M. Lu, X. Huang, T. Li, and D. Xu, 'Application of Gold-Nanoparticle Colorimetric Sensing to Rapid Food Safety Screening', *Sensors*, vol. 18, no. 12, p. 4166, Nov. 2018, doi: 10.3390/s18124166.
[42] Y. Qi, Y. Chen, F.-R. Xiu, and J. Hou, 'An aptamer-based colorimetric sensing of acetamiprid in environmental samples: Convenience, sensitivity and practicability', *Sens. Actuators B Chem.*, vol. 304, p. 127359, Feb. 2020, doi: 10.1016/j.snb.2019.127359.
[43] O. A. Alsager, K. M. Alotaibi, A. M. Alswieleh, and B. J. Alyamani, 'Colorimetric Aptasensor of Vitamin D3: A Novel Approach to Eliminate Residual Adhesion between Aptamers and Gold Nanoparticles', *Sci. Rep.*, vol. 8, no. 1, p. 12947, Dec. 2018, doi: 10.1038/s41598-018-31221-y.
[44] A. Bosak *et al.*, 'Aptamer–gold nanoparticle conjugates for the colorimetric detection of arboviruses and vector mosquito species', *RSC Adv.*, vol. 9, no. 41, pp. 23752–23763, 2019, doi: 10.1039/C9RA02089F.

[45] W. Zhou, W. Kong, X. Dou, M. Zhao, Z. Ouyang, and M. Yang, 'An aptamer based lateral flow strip for on-site rapid detection of ochratoxin A in Astragalus membranaceus', *J. Chromatogr. B*, vol. 1022, pp. 102–108, Jun. 2016, doi: 10.1016/j.jchromb.2016.04.016.
[46] S. Wu, L. Liu, N. Duan, Q. Li, Y. Zhou, and Z. Wang, 'Aptamer-Based Lateral Flow Test Strip for Rapid Detection of Zearalenone in Corn Samples', *J. Agric. Food Chem.*, vol. 66, no. 8, pp. 1949–1954, Feb. 2018, doi: 10.1021/acs.jafc.7b05326.
[47] M. McKeague *et al.*, 'Comparison of In-Solution Biorecognition Properties of Aptamers against Ochratoxin A', *Toxins*, vol. 8, no. 11, p. 336, Nov. 2016, doi: 10.3390/toxins8110336.
[48] M. Jauset-Rubio, M. S. El-Shahawi, A. S. Bashammakh, A. O. Alyoubi, and C. K. O'Sullivan, 'Advances in aptamers-based lateral flow assays', *TrAC Trends Anal. Chem.*, vol. 97, pp. 385–398, Dec. 2017, doi: 10.1016/j.trac.2017.10.010.
[49] S. Srinivasan, V. Ranganathan, M. C. DeRosa, and B. M. Murari, 'Comparison of turn-on and ratiometric fluorescent G-quadruplex aptasensor approaches for the detection of ATP', *Anal. Bioanal. Chem.*, vol. 411, no. 7, pp. 1319–1330, Mar. 2019, doi: 10.1007/s00216-018-1484-x.
[50] L. S. John Ho, R. Fogel, and J. L. Limson, 'Generation and screening of histamine-specific aptamers for application in a novel impedimetric aptamer-based sensor', *Talanta*, vol. 208, p. 120474, Feb. 2020, doi: 10.1016/j.talanta.2019.120474.
[51] R. Velu and M. C. DeRosa, 'Lateral flow assays for Ochratoxin A using metal nanoparticles: comparison of "adsorption–desorption" approach to linkage inversion assembled nano-aptasensors (LIANA)', *The Analyst*, vol. 143, no. 19, pp. 4566–4574, 2018, doi: 10.1039/C8AN00963E.
[52] M. H. Jazayeri, T. Aghaie, A. Avan, A. Vatankhah, and M. R. S. Ghaffari, 'Colorimetric detection based on gold nano particles (GNPs): An easy, fast, inexpensive, low-cost and short time method in detection of analytes (protein, DNA, and ion)', *Sens. Bio-Sens. Res.*, vol. 20, pp. 1–8, Sep. 2018, doi: 10.1016/j.sbsr.2018.05.002.
[53] M. Sabela, S. Balme, M. Bechelany, J.-M. Janot, and K. Bisetty, 'A Review of Gold and Silver Nanoparticle-Based Colorimetric Sensing Assays', *Adv. Eng. Mater.*, vol. 19, no. 12, p. 1700270, Dec. 2017, doi: 10.1002/adem.201700270.
[54] H. Deng, X. Zhang, A. Kumar, G. Zou, X. Zhang, and X.-J. Liang, 'Long genomic DNA amplicons adsorption onto unmodified gold nanoparticles for colorimetric detection of Bacillus anthracis', *Chem Commun*, vol. 49, no. 1, pp. 51–53, 2013, doi: 10.1039/C2CC37037A.
[55] Y. Hong, Y.-M. Huh, D. S. Yoon, and J. Yang, 'Nanobiosensors Based on Localized Surface Plasmon Resonance for Biomarker Detection', *J. Nanomater.*, vol. 2012, pp. 1–13, 2012, doi: 10.1155/2012/759830.
[56] V. Garg *et al.*, 'Localized surface plasmon resonance on Au nanoparticles: tuning and exploitation for performance enhancement in ultrathin photovoltaics', *RSC Adv.*, vol. 6, no. 31, pp. 26216–26226, 2016, doi: 10.1039/C5RA25575A.
[57] K. Shrivas, R. Shankar, and K. Dewangan, 'Gold nanoparticles as a localized surface plasmon resonance based chemical sensor for on-site colorimetric detection of arsenic in water samples', *Sens. Actuators B Chem.*, vol. 220, pp. 1376–1383, Dec. 2015, doi: 10.1016/j.snb.2015.07.058.
[58] W. Haiss, N. T. K. Thanh, J. Aveyard, and D. G. Fernig, 'Determination of Size and Concentration of Gold Nanoparticles from UV−Vis Spectra', *Anal. Chem.*, vol. 79, no. 11, pp. 4215–4221, Jun. 2007, doi: 10.1021/ac0702084.

[59] M. E. Stewart *et al.*, 'Nanostructured Plasmonic Sensors', *Chem. Rev.*, vol. 108, no. 2, pp. 494–521, Feb. 2008, doi: 10.1021/cr068126n.
[60] P. Nordlander, C. Oubre, E. Prodan, K. Li, and M. I. Stockman, 'Plasmon Hybridization in Nanoparticle Dimers', *Nano Lett.*, vol. 4, no. 5, pp. 899–903, May 2004, doi: 10.1021/nl049681c.
[61] V. S. Godakhindi *et al.*, 'Tuning the Gold Nanoparticle Colorimetric Assay by Nanoparticle Size, Concentration, and Size Combinations for Oligonucleotide Detection', *ACS Sens.*, vol. 2, no. 11, pp. 1627–1636, Nov. 2017, doi: 10.1021/acssensors.7b00482.
[62] T. Yu *et al.*, 'Aptamer based high throughput colorimetric biosensor for detection of staphylococcus aureus', *Sci. Rep.*, vol. 10, no. 1, p. 9190, Dec. 2020, doi: 10.1038/s41598-020-66105-7.
[63] X. Hu, K. Chang, S. Wang, X. Sun, J. Hu, and M. Jiang, 'Aptamer-functionalized AuNPs for the high-sensitivity colorimetric detection of melamine in milk samples', *PLOS ONE*, vol. 13, no. 8, p. e0201626, Aug. 2018, doi: 10.1371/journal.pone.0201626.
[64] J. Lee, C. H. Jeon, S. J. Ahn, and T. H. Ha, 'Highly stable colorimetric aptamer sensors for detection of ochratoxin A through optimizing the sequence with the covalent conjugation of hemin', *The Analyst*, vol. 139, no. 7, pp. 1622–1627, 2014, doi: 10.1039/C3AN01639K.
[65] C. Entzian and T. Schubert, 'Studying small molecule–aptamer interactions using MicroScale Thermophoresis (MST)', *Methods*, vol. 97, pp. 27–34, Mar. 2016, doi: 10.1016/j.ymeth.2015.08.023.
[66] 'OligoAnalyzer Tool - primer analysis | IDT', *Integrated DNA Technologies*. https://www.idtdna.com/pages/tools/oligoanalyzer (accessed Nov. 24, 2020).
[67] C. Platella, C. Riccardi, D. Montesarchio, G. N. Roviello, and D. Musumeci, 'G-quadruplex-based aptamers against protein targets in therapy and diagnostics', *Biochim. Biophys. Acta BBA - Gen. Subj.*, vol. 1861, no. 5, pp. 1429–1447, May 2017, doi: 10.1016/j.bbagen.2016.11.027.
[68] C. Roxo, W. Kotkowiak, and A. Pasternak, 'G-Quadruplex-Forming Aptamers—Characteristics, Applications, and Perspectives', *Molecules*, vol. 24, no. 20, p. 3781, Oct. 2019, doi: 10.3390/molecules24203781.
[69] J. A. Capra, K. Paeschke, M. Singh, and V. A. Zakian, 'G-Quadruplex DNA Sequences Are Evolutionarily Conserved and Associated with Distinct Genomic Features in Saccharomyces cerevisiae', *PLoS Comput. Biol.*, vol. 6, no. 7, p. 13, 2010.
[70] S. Hu, P.-J. J. Huang, J. Wang, and J. Liu, 'Dissecting the Effect of Salt for More Sensitive Label-Free Colorimetric Detection of DNA Using Gold Nanoparticles', *Anal. Chem.*, vol. 92, no. 19, pp. 13354–13360, Oct. 2020, doi: 10.1021/acs.analchem.0c02688.
[71] R. Wu, L.-P. Jiang, J.-J. Zhu, and J. Liu, 'Effects of Small Molecules on DNA Adsorption by Gold Nanoparticles and a Case Study of Tris(2-carboxyethyl)phosphine (TCEP)', *Langmuir*, vol. 35, no. 41, pp. 13461–13468, Oct. 2019, doi: 10.1021/acs.langmuir.9b02652.
[72] F. Zhang, S. Wang, and J. Liu, 'Gold Nanoparticles Adsorb DNA and Aptamer Probes Too Strongly and a Comparison with Graphene Oxide for Biosensing', *Anal. Chem.*, vol. 91, no. 22, pp. 14743–14750, Nov. 2019, doi: 10.1021/acs.analchem.9b04142.
[73] T. H. Scheuermann, S. B. Padrick, K. H. Gardner, and C. A. Brautigam, 'On the acquisition and analysis of microscale thermophoresis data', *Anal. Biochem.*, vol. 496, pp. 79–93, Mar. 2016, doi: 10.1016/j.ab.2015.12.013.

[74] B. O'Farrell, 'Lateral Flow Immunoassay Systems', in *The Immunoassay Handbook*, Elsevier, 2013, pp. 89–107.
[75] G. Zhang, C. Zhu, Y. Huang, J. Yan, and A. Chen, 'A Lateral Flow Strip Based Aptasensor for Detection of Ochratoxin A in Corn Samples', *Molecules*, vol. 23, no. 2, p. 291, Jan. 2018, doi: 10.3390/molecules23020291.